Progress in Atomic Fountains at LNE-SYRTE

Jocelyne Guéna, Michel Abgrall, Daniele Rovera, Philippe Laurent, Baptiste Chupin, Michel Lours, Giorgio Santarelli, Peter Rosenbusch, Michael E. Tobar, Ruoxin Li, Kurt Gibble, Andre Clairon, and Sebastien Bize

(*Invited Review*)

***Abstract*—We give an overview of the work done with the Laboratoire National de Métrologie et d'Essais–Systèmes de Référence Temps-Espace (LNE-SYRTE) fountain ensemble during the last five years. After a description of the clock ensemble, comprising three fountains, FO1, FO2, and FOM, and the newest developments, we review recent studies of several systematic frequency shifts. This includes the distributed cavity phase shift, which we evaluate for the FO1 and FOM fountains, applying the techniques of our recent work on FO2. We also report calculations of the microwave lensing frequency shift for the three fountains, review the status of the blackbody radiation shift, and summarize recent experimental work to control microwave leakage and spurious phase perturbations. We give current accuracy budgets. We also describe several applications in time and frequency metrology: fountain comparisons, calibrations of the international atomic time, secondary representation of the SI second based on the ^{87}Rb hyperfine frequency, absolute measurements of optical frequencies, tests of the T2L2 satellite laser link, and review fundamental physics applications of the LNE-SYRTE fountain ensemble. Finally, we give a summary of the tests of the PHARAO cold atom space clock performed using the FOM transportable fountain.**

I. Introduction

Atomic fountain clocks provide the most accurate realization of the SI second and define the accuracy of international atomic time (TAI). Ten years ago, a few formal TAI calibration reports were available each year. Now, there are normally several formal reports each month as a result of a great deal of effort at several metrology institutes to improve reliability and long-term operation. At Laboratoire National de Métrologie et d'Essais–Systèmes de Référence Temps-Espace (LNE-SYRTE), the fountain ensemble typically provides more than 20 TAI calibrations each year, about half of all reports. These large improvements in reliability and the corresponding capability to perform lengthy measurements yield an enhanced ability to investigate smaller and smaller frequency shifts, to compare fountain clocks with more stringent uncertainties, and to test their long-term behavior. In turn, applications using atomic fountain clocks have also developed and benefited from the improvements of the last few years.

In this article, we give an overview of developments and of applications of the LNE-SYRTE atomic fountain ensemble during the last five years.

Manuscript received September 15, 2011; accepted January 23, 2012. This work was supported by Systèmes de Référence Temps-Espace (SYRTE), the Laboratoire National de Métrologie et d'Essais (LNE), the Centre National de la Recherche Scientifique (CNRS), Université Pierre et Marie Curie (UPMC), the Observatoire de Paris, the Institut Francilien de Recherche sur les Atomes Froids (IFRAF), the National Science Foundation (NSF), Penn State, the Ville de Paris, the European Space Agency (ESA), and the Centre National d'Etudes Spatiales (CNES).

J. Guéna, M. Abgrall, D. Rovera, P. Laurent, B. Chupin, M. Lours, G. Santarelli, P. Rosenbusch, A. Clairon, and S. Bize are with LNE-SYRTE, Observatoire de Paris, CNRS, UPMC, Paris, France (e-mail: sebastien.bize@obspm.fr).

M. E. Tobar is with The School of Physics, University of Western Australia, Crawley, Australia.

R. Li and K. Gibble are with The Department of Physics, The Pennsylvania State University, University Park, PA.

DOI: http://dx.doi.org/10.1109/TUFFC.2012.2208

II. The LNE-SYRTE Fountain Ensemble

A. Overview

LNE-SYRTE has operated three atomic fountains for more than a decade. The first, FO1, is a ^{133}Cs fountain which has been in operation since 1994 [1]. The second, FOM, was originally a prototype for the Projet d'Horloge Atomique par Refroidissement d'Atomes en Orbite (PHARAO) cold atom space clock [2] and was later modified to be a transportable fountain clock. The third, FO2, is a dual fountain which operates with ^{87}Rb and ^{133}Cs simultaneously [3]. Development over more than a decade has continuously improved each of these. Our description here reflects the present configuration.

The three fountains share several features. All of them are gathering atoms in a Lin $\perp$ Lin optical molasses with laser beams oriented to launch atoms vertically in the so-called (1,1,1) configuration[1] [4]. The 6 laser beams for the optical molasses are obtained from 6 fiber-coupled collimators, which are designed, machined, and tuned to ensure proper alignment at the level of a few hundred microrads when placed against the corresponding reference surfaces of the vacuum chamber. Similar fiber-coupled collimators provide the other laser beams for state selection and detection. In all three fountains, including the ^{87}Rb part of FO2, the laser system is on a separate optical bench and the light is coupled to the vacuum system with optical fibers. The lasers are home-built extended-cavity diode lasers, most of which use a narrowband interference filter for wavelength selection [5]. This design is used in the

[1] In this configuration, the 3 pairs of counter-propagating laser beams for the molasses are aligned along the axes of a 3-dimensional orthonormal basis, where the (111) direction is along the vertical direction, as shown in Fig. 2.

PHARAO cold atom space clock (see Section VI). It has also recently become commercially available. The required power is obtained either by injection locking another laser diode or using a tapered semi-conductor laser amplifier. In all three fountains, atoms are launched with the moving molasses technique [6] at a velocity of ~4 m·s^{-1} and a temperature of ~1μK. Atoms exit the launch sequence in the upper hyperfine state. For normal clock operation, microwave and laser pulses further select the atoms in the $m_F = 0$ Zeeman sub-state of the lower hyperfine state ($|F = 3, m_F = 0\rangle$ for ^{133}Cs, $|F = 1, m_F = 0\rangle$ for ^{87}Rb).

All three fountains also have at least one layer of magnetic shielding that surrounds the entire vacuum system. Notably, the molasses and the detection region are shielded, which is important to operate in the presence of the strong magnetic field fluctuations found in many urban environments, including the Observatoire de Paris. The largest, vertical magnetic field component in the lower part of the fountain (molasses and detection) is measured by a flux-gate magnetometer and actively stabilized with a set of horizontal coils distributed over the height of the fountain. Two or three additional cylindrical shields with end caps surround only the interrogation region to further attenuate magnetic field fluctuations. Inside the innermost shield, a solenoid and a set of compensation coils provide a static magnetic field in the range of 80 to 200 nT. The field is homogeneous to 10^{-3} and stable to 2×10^{-5} from 1 s to several days, as established by spectroscopy of the $|F, m_F = 1\rangle \rightarrow |F + 1, m_F = 1\rangle$ field-sensitive transition. This corresponds to a stability of ~4 pT.

All three fountains also use the same strategy to control temperature and thermal gradients in the interrogation region. The innermost layer surrounding the interrogation is made of a material with high thermal conductivity (copper or aluminum alloy) and is well isolated from the environment to ensure good temperature uniformity of this layer. The temperature of this innermost layer is monitored using platinum resistors and is allowed to drift slowly, following temperature fluctuations in the room with a typical time constant of 1 day. The measured temperature is used to infer the blackbody radiation temperature seen by the atoms. With this scheme, the temperature of the innermost layer is uniform to much better than 0.1K and no large gradients exist between the inner region and the environment. This essentially removes concerns about the effect of the necessary openings (for the atomic trajectories, pumping, etc.) on the effective blackbody temperature for the atoms. Using heating devices to change or actively stabilize the temperature of the innermost layer induced a significant degradation of the temperature uniformity, which was difficult to compensate, even with segmented heaters. Consequently, this approach was abandoned.

The microwave interrogation cavities in all three fountains are TE_{011} copper resonators with two independent microwave feedthroughs. The microwave synthesizers used to feed the cavities are home-built. Despite significant differences, these synthesizers are all capable of using the ultra-low phase noise reference signal (see Section II-E) from a cryogenic sapphire oscillator (CSO) without significant degradation at the level of one to a few parts in 10^{15} at 1 s [7]. Consequently, the short-term instability of all three fountains is typically limited by the atomic quantum projection noise [8] and technical noise in the atom detection. The best short-term stability to date for the operation of an atomic fountain with a high atom number is $1.6 \times 10^{-14}\tau^{-1/2}$ as reported in [9] and exemplified in Fig. 1. The present versions of the synthesizers also incorporate a phase-stable microwave switch [10] which helps to assess and remove leakage fields that may affect the interrogation process, independent of other systematic effects. Some details are given in Section III-D.

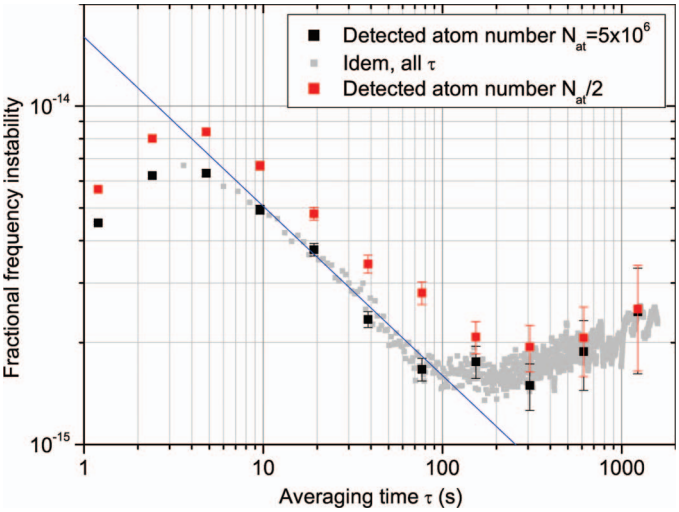

Fig. 1. Fractional frequency instability of the FO2-Cs fountain when using a cryogenic sapphire oscillator as a reference signal. The black points are obtained for a high atom number: $N_{at} = 5 \times 10^6$ detected atoms. The red points are obtained for $N_{at}/2$ detected atoms. The blue line corresponds to $1.6 \times 10^{-14}\tau^{-1/2}$. Above 100 s, frequency fluctuations of the ultra-stable interrogation signal (see Section II-E), common to the high and low atom number measurements, are apparent.

For all three fountains, the computer system allows automated control of most of the important parameters, enabling routine implementation of multiple interleaved measurements with different configurations to study systematic shifts. A large number of parameters (laser powers, temperatures in the interrogation region, temperatures in the environment, at the Cs or Rb sources, humidity, etc.) are frequently monitored. The microwave power is regularly optimized and the magnetic field is verified via spectroscopy of a field-sensitive transition, with automated computer-controlled sequences.

B. FO1

FO1 uses a 2-dimensional magneto-optical trap (2DMOT) [11] as a source of slow atoms to load the optical molasses. An advantage of this type of source is that it confines the high alkali vapor pressure to the 2DMOT chamber, yielding a large number of cold atoms in the molasses while keeping source consumption low. It also facilitates a better vacuum in the molasses region, there-

by minimizing perturbations in the detection region and the contamination of the interrogation, including the microwave cavity, by background alkali vapor. With higher laser powers in the 2DMOT, it should be possible to reproduce the atom numbers previously obtained with a chirped-slowed thermal atomic beam that gave the best reported fountain stability [9], while consuming less alkali metal by an order of magnitude. So far, the laser power devoted to the 2DMOT yields ~1/4 the number of atoms in the molasses than does our best chirped-cooled atomic beam. Note that 2DMOT loading of the molasses has some disadvantages. Besides the quite intricate mechanical and optical design and the need for extra laser sources, we observe a degradation of the 2DMOT laser windows that are in contact with the relatively high alkali vapor pressure (up to 10^{-4} Pa) after a few years of almost continuous operation. Also, loading the molasses asymmetrically from the slow atom beam from the 2DMOT leads to a non-spherical, complicated atomic cloud distribution which makes the investigation of some systematic frequency shifts more difficult. Note, however, that by using the adiabatic passage method to change the atom number [12], the extrapolation of the cold collision shift to zero density is essentially unaffected by distortions of the atomic cloud's shape.

The microwave cavity in FO1 has a diameter of 42.99 mm and a length of 42.88 mm. The below-cutoff guides that let the atoms pass through the cavity have a diameter of 12 mm and a length of 60 mm. At the two ends of the cutoff guides, an additional diaphragm with a diameter of 11 mm blocks atoms that could travel close to the copper walls. Each of the 2 opposing microwave feedthroughs includes a resonant, polarization-filtering rectangular waveguide section. In the latest implementation, the cavity has a loaded quality factor of 14 000.

The interrogation region in FO1 is currently equipped with Stark plates. These can be used to measure the sensitivity of the clock transition to static electric fields to determine the Stark coefficient for the blackbody radiation shift correction. Alternatively, FO1 can be equipped with a blackbody radiator to directly measure the blackbody radiation shift (see Section III-C).

C. FO2 Dual Rb/Cs Fountain

A schematic view of the FO2 dual Rb/Cs fountain is shown in Fig. 2. It uses 2 independent 2DMOT sources for Cs and for Rb. For Cs, the 2DMOT eliminates the Cs background atoms. For Rb, only the 27.8% abundant isotope is used in the fountain and the use of a 2DMOT eliminates the ^{87}Rb background atoms and also the larger background from the unwanted ^{85}Rb isotope. The Rb and Cs molasses are superimposed with dichroic collimators for each molasses beam, where the 852-nm light (Cs) and the 780-nm light (Rb) come from 2 independent optical benches through polarizing fibers and are then combined with a dielectric dichroic beamsplitter and collimated with an achromatic lens [13]. Similar dichroic collimators are used for all other laser beams, the pushing beam for the state selection, detection beams, and repumper for detection.

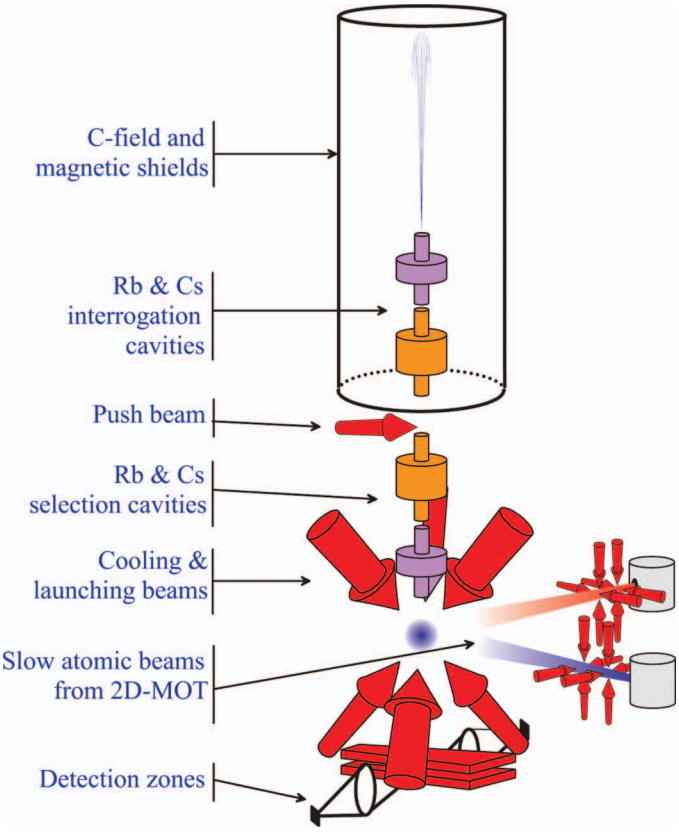

Fig. 2. Schematic view of the FO2 dual Rb/Cs fountain. The 852-nm light and the 780-nm light for ^{133}Cs and ^{87}Rb atoms are superimposed in each of the 9 laser beams with dichroic beam splitters. ^{133}Cs and ^{87}Rb atoms are captured, launched, state-selected, probed, and detected simultaneously at each fountain cycle of 1.6 s. There are 2 independent 2-D magneto-optic traps for the 2 atomic species.

As shown in Fig. 2, there are a total of 4 microwave cavities for state selection and interrogation of Rb and Cs atoms. Because both interrogation cavities are in the interrogation region, their temperature must be uniform and therefore the same as the environment temperature, which removes any possibility to independently tune each cavity. Practically, the Rb and Cs cavities are a single copper assembly where the Rb and Cs cavity resonances were mechanically tuned relative to one another, after a lengthy and tedious process. The resonance frequencies had to be verified under vacuum and tightly controlled thermal conditions, after each tuning step that was a controlled polishing of the two cavity spacers [14], [15]. The Rb and Cs microwave cavities have the same aspect ratio, with the radii scaled by the ratio of the hyperfine frequencies. The cavity for Cs is located at the top. It has a diameter of 50.00 mm and a length of 26.87 mm. The Rb cavity has a diameter of 67.25 mm and a length of 36.01 mm. The below-cutoff end cap tubes have a diameter of 12 mm and a length of ~50 mm. The 2 opposing microwave feedthroughs for each cavity include a reso-

nant, polarization filtering rectangular waveguide section. The loaded quality factor is 7000 for Cs and 6000 for Rb.

The Rb and Cs clocks in FO2 have routinely operated simultaneously since 2009 [3]. Two independent but connected and synchronized computer systems allow the coordination of multiple interleaved measurements with Cs and Rb, as well as all other tasks for each clock, such as monitoring the temperature, the magnetic field, etc. Thus far, the nominal configuration is to launch the Rb and Cs clouds almost simultaneously, but at different velocities, so that the interrogation times are simultaneous, i.e., the Rb cloud is at the center of the Rb cavity when the Cs cloud is at the center of the Cs cavity, on both the way up and the way down. In this way, the two atomic clouds do not interact with each other during the interrogation process, avoiding interspecies collisions. The two clouds also remain well separated as they fall to the detection region, allowing the time-resolved detection of Rb and Cs [3]. As a result, the Rb and Cs clocks run simultaneously without impacting the performance of the other. The flexible computer systems allow for a large number of other possibilities which will be explored in the future. For instance, one cloud can be purposely launched through the other with a well controlled and yet variable speed, to study interspecies collisions at varying energies [16], based either on measurements of the cold collision frequency shift or on direct detection of the scattered wave [17].

D. FOM Transportable Fountain

Photographs of the transportable fountain FOM are shown in Fig. 3. FOM has two major subsystems. The first is the vacuum system where atoms are manipulated. The second is the optical laser bench, its electronics, the microwave synthesizer, and the computer system that operates the fountain, all of which are mounted on a single frame. Both of these subsystems include vibration damping devices necessary for transportation. When disconnected, the two subsystems fit into a small truck. A battery powers the ion pump to maintain the vacuum of the system. After transportation, the two subsystems are reconnected (polarizing optical fibers for the laser light, microwave cables, wires for monitoring) and the system is allowed to thermally stabilize for a few hours. After a limited number of manual re-optimizations (laser power through the optical fibers), a computer-controlled sequence is started which automatically finds the laser set points and activates the laser-stabilization loops [18]. At remote locations, close-to-nominal operation of the fountain is typically achieved in less than 2 days.

One notable feature of the transportable fountain FOM is that the microwave synthesizer has two possible modes of operation. At LNE-SYRTE and at laboratories where a high-quality metrological reference signal is available, the microwave synthesizer is synchronized to this external reference and the FOM fountain works as a frequency standard calibrating the frequency of the external reference. In the second configuration, FOM autonomously delivers a primary reference signal. Here, a BVA quartz oscillator synchronizes the microwave synthesizer and a digital loop locks the frequency of this BVA quartz oscillator to the atoms.

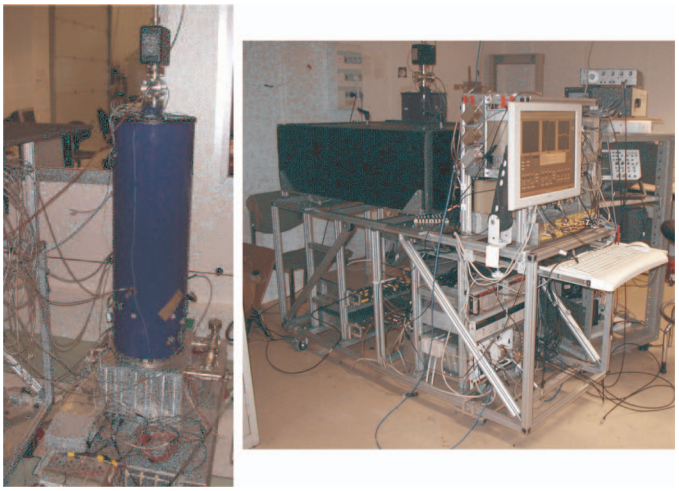

Fig. 3. Pictures of the transportable fountain FOM. On the left is the vacuum chamber for cooling and launching cesium atoms. Four layers of magnetic shielding surround the chamber. On the right is the second clock component with (on top) the optical bench inside an acoustic box, and (below the box) the electronics, including the microwave synthesis chain. A computer controls the clock.

The microwave interrogation cavity in FOM has a diameter of 41.06 mm and a length of 65.66 mm. The two opposing microwave feedthroughs have direct evanescent coupling: the coaxial input cable is terminated in a small non-resonant cavity, with an antenna located a few millimeters away from the coupling iris of the cavity. The cavity has a loaded quality factor of 21 000.

E. Ultra-Stable Reference and Frequency Distribution Scheme

Fig. 4 is a schematic diagram of the LNE-SYRTE fountain ensemble. A CSO [19], [20] is the local oscillator for all of the atomic fountains. Its ultra-low phase noise allows the fountains to operate at the quantum projection noise limit [8], producing short-term instabilities as low as 1.6×10^{-14} at 1 s ([9] and Fig. 1). As shown in Fig. 4, a finely tunable[2] microwave 11.98-GHz signal is first derived from the free-running CSO. This frequency is divided down to 100 MHz and compared with the output of one of the LNE-SYRTE hydrogen masers, H1 in Fig. 4. A computer-driven digital phase-locked loop (time constant ~1000 s) corrects the frequency of the 11.98-GHz microwave signal to phase lock the 100-MHz signals. This 11.98-GHz reference has the exquisite phase noise properties of the CSO for time scales less than ~1000 s and the mid- and long-term frequency stability of the hydrogen maser, while providing the connection to LNE-SYRTE timescales, to TAI, and to other laboratories via Global Positioning System

[2] With a computer controlled direct digital synthesizer.

(GPS) and two-way satellite time and frequency transfer (TWSTFT). This 11.98-GHz signal is the high-performance reference from which all other signals are derived. A 1-GHz source is the starting point of the microwave synthesis for FO1, FO2-Rb, and FOM. Because FO2 is located next door to the CSO, a more direct synthesis from 11.98 to 9.192 GHz could be used for FO2-Cs [21]. To compare with optical clocks through optical frequency combs, an 8.985-GHz signal is also generated. Finally, an additional synthesizer generates signals in the 6 to 9 GHz range for testing (see Section III-D). The design and characterization of the low-phase-noise electronics that generate these reference signals are reported in [7], [21]. Phase noise power spectral densities can be found in [20] for the CSO alone, and in [7], [21], and [22] for the derived reference signals.

Fig. 4 shows 100- to 300-m-long actively compensated optical fiber links that are used to distribute the reference signals. These links are simplified versions of similar long-distance links [23] because of the short distance and limited insertion losses. The reference signal modulates the current of a 1.55-μm diode laser that is launched into a standard telecom fiber. At the remote end, a fast photodiode detects the intensity modulation and delivers the signal to the application. A fraction of this recovered signal is used to modulate a second diode laser that is launched back into the fiber. At the emission site, the returned signal is detected by another fast photodiode and then mixed with the reference signal to detect the phase variations imposed by the two propagation passes through the fiber. A temperature-controlled fiber spool of 50 to 100 m is inserted to control the length of the link to cancel these phase variations with a computer operated servo-loop (time constant ~10 s). For the high-performance links at 6 to 9 GHz and 8.985 GHz, an additional fast actuated piezo-driven fiber stretcher is used (bandwidth ~400 Hz). Characterization of these links has shown stabilities $\sim 10^{-14}$ at 1 s for the 1-GHz carrier and $\sim 2 \times 10^{-15}$ at 1 s for the 6 to 9 GHz and 8.985-GHz carriers, and a residual frequency offset well below 10^{-16}. A computer acquires and analyzes the double-passed phase signals to assess the performance in real-time and detect anomalies.

F. New Solution for the Ultra-Low Noise Reference Oscillator

The CSO allows a large improvement in the fountain short-term stability but requires cumbersome and costly liquid helium refills every 26 days. Each refill lasts several hours and degrades the performance of the CSO for nearly half a day. An alternate solution for fully continuous operation of an ultra-low noise microwave reference would be to use a pulsed-tube cryocooler for the CSO [24]–[27]. However, advances in laser frequency stabilization and optical frequency combs offer the possibility of replacing the CSO with a fully continuous, cryogen-free and maintenance-free ultra-low-noise microwave generation system.

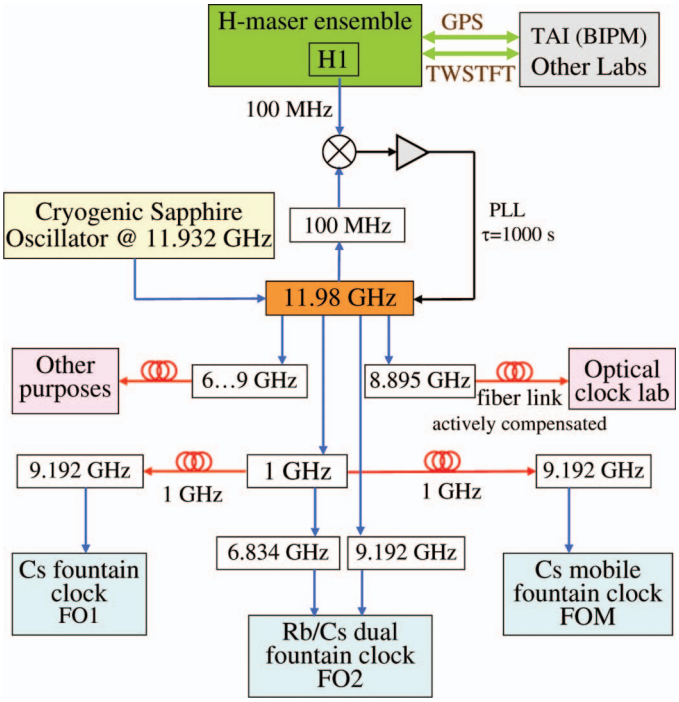

Fig. 4. LNE-SYRTE clock ensemble. A cryogenic sapphire oscillator generates an ultra-low noise reference signal that is distributed to all three fountains. This 11.98-GHz reference signal is slowly phase-locked (PLL) to the output of a hydrogen maser (H1), which provides long-term stability and the connection to local timescales, satellite time-transfer systems (GPS, TWSTFT), and international atomic time (TAI). The reference signal can also be distributed through actively compensated fiber links.

Fig. 5 shows a schematic of such a laser-based system. An ultra-stable laser is realized by stabilizing a reliable 1.55-μm laser, such as an erbium-doped fiber laser or an extended cavity laser, to an ultra-stable reference Fabry-Perot cavity. Several Fabry-Perot stabilized lasers have demonstrated short-term stabilities well below 10^{-15} [28]–[30], similar to stabilities reported for cryogenic sapphire oscillators [20]. Note, however, that simplified versions of these cavities can be sufficient for application to atomic fountains. Microwave signals with short-term frequency stabilities in the mid 10^{-15} range at 1 s are indeed sufficient to achieve the quantum projection noise limit at 10^{-14} at 1 s. This instability is not easy to surpass for other reasons: it is difficult to increase the number of useful atoms per cycle, to cope with the tremendous cold collision shift that would result from more atoms, and to suppress certain detection noise sources. A short ($\leq$10 cm) reference Fabry-Perot cavity with mirrors made of ultra-low-expansion glass with a comparatively simple temperature stabilization system can deliver instabilities less than 2×10^{-15} between 1 and 1000 s, which is well suited to atomic fountains.

As shown in Fig. 5, the ultra-stable laser is used to stabilize the repetition rate of the optical frequency comb generated by a fiber-based femtosecond laser. A well-chosen harmonic, here 12 GHz, is detected and divided down

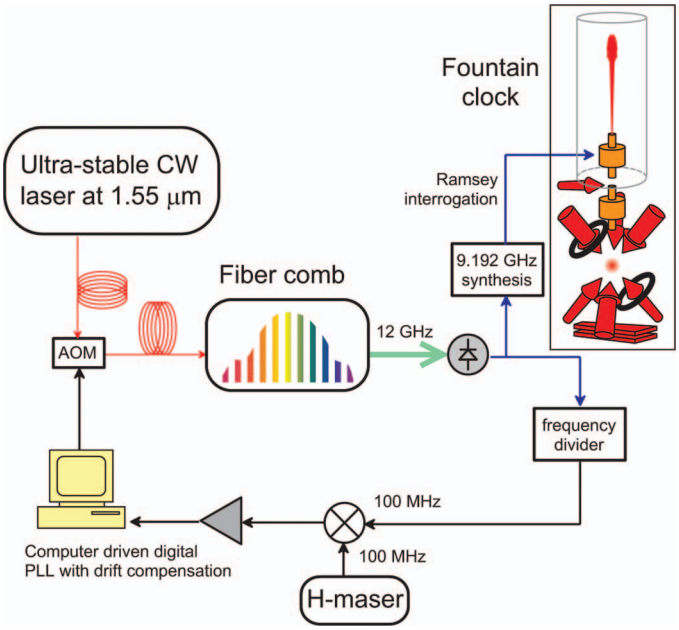

Fig. 5. An ultra-stable laser and an optical frequency comb produce an ultra-low noise microwave flywheel for the atomic fountains. The 12-GHz microwave signal is obtained by detecting a harmonic of the repetition rate of an Er-doped fiber femtosecond laser, which is stabilized to a continuous wave (CW) laser, itself stabilized to an ultra-stable Fabry-Perot cavity.

to 100 MHz to allow a phase comparison with a hydrogen maser, similar to what is done for the CSO (see Section II-E). Here, a digital phase-locked loop shifts the frequency of the acousto-optic modulator (AOM) and thereby the ultra-stable light that controls the comb repetition rate, ensuring the long-term stability of the 12-GHz reference that ultimately provides the 9.192-GHz interrogation signal for the fountains.

Ultra-low noise microwave generation with fiber-based optical frequency combs was demonstrated in [31] and [32]. Atomic fountains using microwave signals derived from optical references reported fountain short-term stabilities of $3.5 \times 10^{-14}\tau^{-1/2}$ [33] and $7.4 \times 10^{-14}\tau^{-1/2}$ [34]. For both, the fountain stability was limited by quantum projection noise, and the microwave signal alone was compatible with a fountain stability $\leq 10^{-14}\tau^{-1/2}$. Subsequent progress on fiber-based optical frequency combs will enable the implementation of a fully operational version of the system of Fig. 5.

An alternative approach for achieving quantum noise limited stability without an ultra-low-noise microwave source is the continuous atomic fountain [35], [36].

III. Recent Studies of Systematic Shifts

A. Distributed Cavity Phase Shift

The distributed cavity phase (DCP) shift is a residual first-order Doppler shift that occurs when the moving atoms interact with the field inside the microwave cavity that has a spatial phase variation. Until recently, measurements were unable to reveal this effect and to reasonably agree with calculations. The corresponding frequency shifts can be quite small, the measured frequency shifts give only indirect information about the phase variations, and this shift and its changes with fountain parameters can be intermingled with other systematic effects. Also, accurately calculating the actual phase distribution and its corresponding frequency shift was a challenging numerical problem.

In [37] and [38], a new theoretical approach was proposed to solve the problem of the cavity field computation. The field, represented explicitly as the sum of a large standing wave $\mathbf{H}_0(\mathbf{r})$ and a small field, $\mathbf{g}(\mathbf{r}) = \sum \mathbf{g}_m(\rho, z)\cos(m\phi)$, which describes the effects of wall losses and cavity feeds, is expressed as an azimuthal Fourier series. Only the lowest azimuthal terms are relevant: $m = 0$, $m = 1$, and $m = 2$. We have recently published measurements of the DCP shift performed with ^{133}Cs in FO2 [39] where, for the first time, quantitative agreement between theory and experiment is found. This study led to a better characterization and a quantitative evaluation of the contributions to the uncertainty of the DCP shift. It highlighted the importance of controlling the fountain geometry, notably the effective tilt of the fountain and the detection inhomogeneity, to reduce the DCP shift uncertainty. Based on the experimentally validated model, new cavity designs were proposed [38] to reduce the DCP shift and its uncertainty. These measurements lowered the DCP shift uncertainty for FO2-Cs clock from 3×10^{-16} to 8.4×10^{-17} and defined a set of measurements to establish the DCP uncertainty of a fountain, an approach adopted in [40], [41]. Here, we apply this approach to evaluate the DCP uncertainty of FO1, FOM, and FO2-Rb.

The $m = 1$ term corresponds to power flowing horizontally from one side of the cavity to the other. This contribution can be probed by measuring the fountain frequency as a function of the tilt of the launch direction. The uncertainty for this term is determined by the experimental uncertainty in frequency change as a function of tilt, after correctly balancing the feeds to null the tilt sensitivity, and by the uncertainty of the fountain tilt for nominal operation [39]. When we purposely exaggerate the $m = 1$ DCP shifts by asymmetrically feeding the cavities of FO1 and FOM, the measurements show tilt sensitivities that are much smaller than those of FO2-Cs. This is largely due to the higher quality factor of their cavities and to their smaller cavity apertures.

Also, when the two feeds are adjusted to produce equal Rabi pulse areas, FO1 and FOM show no measured tilt sensitivities at the level of $(1.5 \pm 1.7) \times 10^{-16}$ mrad^{-1} and $(1.8 \pm 1.1) \times 10^{-16}$ mrad^{-1}, respectively, along the axis of the feeds. For FO2-Rb, this sensitivity is $(1.8 \pm 1) \times 10^{-16}$ mrad^{-1}.

Tilt sensitivities in the perpendicular direction remain to be measured for FO1 and FOM. Based on the findings of [39], we can reasonably apply, for the time

being, the same bound as in the parallel direction. For FO2-Rb, the measured perpendicular sensitivity is $\leq 0.9 \times 10^{-16}$ mrad^{-1}. Using the same methods used in [39] (detected atoms versus tilt, frequency difference between the 2 asymmetric feedings), we estimate the uncertainty on the effective launch direction to be 1 mrad for FO1, 0.2 mrad for FO2-Rb, and 0.7 mrad for FOM in the direction of the feeds, and 0.7 mrad, 0.7 mrad, and 0.7 mrad in the direction perpendicular to the feeds.

The $m = 0$ and $m = 2$ terms are calculated from the phase distributions [37], [38] and the corresponding response of the fountain. This second step takes as an input several parameters of the fountain geometry such as the cloud size, the cloud temperature, and the geometry of the detection. Fig. 6 shows the measured contrast of the Rabi oscillations at upward and downward passages in the microwave cavity, which is used to ascertain the fountain geometry to compute the DCP shift [39]. The same curve, measured for FO2-Cs, is shown in [42].

The resulting DCP shift corrections and their uncertainties are presented in Table I. Several of these uncertainties are expected to decrease when improved measurements of the tilt sensitivities and tilt uncertainties becomes available.

B. Microwave Lensing

The external degrees of freedom of the atoms evolve dynamically during the Ramsey interrogation. The interaction of the atoms with the standing-wave field in the microwave cavity on the upward passage slightly modifies the atomic motion, leading to a predicted shift of the clock frequency. This effect was first called the microwave recoil [43], connecting to the simple situation in which an atom interacts with a plane wave as in optical spectroscopy [44]. In the optical case, an atom absorbs a photon from a plane wave. The shift, expressed in energy, is $(\hbar k)^2/(2m_{\mathrm{at}})$, corresponding to the kinetic energy of the atom with the momentum $\hbar k$ of the absorbed photon. For microwave photons, the corresponding fractional frequency shift is 1.5×10^{-16} for ^{133}Cs, comparable to the best reported fountain accuracy.

In 2006, a new approach to calculating this effect provided better physical insight and made the calculations tractable to treat both transverse dimensions [45]. The microwave standing wave and its spatially varying field amplitude produces a radial magnetic dipole force which acts as a lens to focus (or defocus) the atomic wave packets, hence the name microwave lensing frequency shift. To calculate the shift with reasonable accuracy, it is crucial to properly treat the apertures in the fountain. They truncate the downwardly traveling atomic cloud, and this introduces a difference between the two dressed states, which experience opposite lensing deflections on the upward cavity traversal.

Here, we report calculations of the microwave lensing for the LNE-SYRTE fountains. We apply the approach

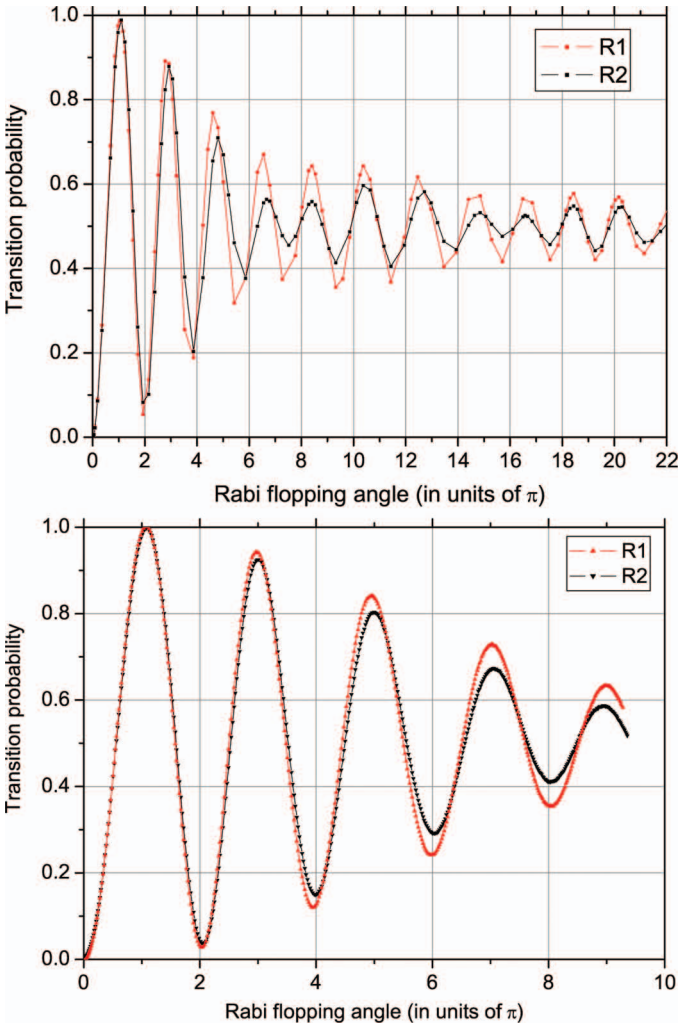

Fig. 6. Measured transition probabilities for resonant Rabi pulses on the upward (R1) and downward (R2) cavity traversals, as a function of the microwave amplitude of (top) FO1 and (bottom) FOM.

that was recently used to evaluate the NPL-CsF2 and PTB-CSF2 fountains [40] [41]. The results are summarized in Table II. The simple analytic result [40] (first line in Table II) neglects all apertures on the upward passage and only treats dipole energy that is quadratic ($\propto \rho^2$) in the radial coordinate ρ. Because the initial clouds in the LNE-SYRTE fountains are not point-like sources, this overestimates the microwave lensing shift because it includes atoms that would be cut by the cavity apertures, which experience much larger dipole forces away from the cavity axis. Including an aperture at the first cavity passage eliminates these atoms from the calculation, giving a smaller and more realistic shift (second line in Table II). Adding the lowest cutoff aperture for the upward passage, the variation of the Rabi tipping angles, and the all-order dipole forces (beyond ρ^2), gives a small correction (third line), as does including the detection inhomogeneities and imperfect Ramsey fringe contrast, yielding the predicted shift.

TABLE I. CORRECTIONS AND THEIR UNCERTAINTIES FOR THE DISTRIBUTED CAVITY PHASE (DCP) SHIFT IN FO1, FO2, AND FOM, IN UNITS OF 10^{-17}.

m	FO1	FO2-Cs	FOM	FO2-Rb	Source
0	-0.7 ± 0.4	-0.4 ± 0.2	-1.5 ± 0.7	-0.2 ± 0.1	Homogeneous wall losses
	0 ± 0.8	0 ± 0.7	0 ± 1.2	0 ± 0.5	20% top/bottom loss asymmetry
	-0.7 ± 0.9	-0.4 ± 0.8	-1.5 ± 1.4	-0.2 ± 0.5	Total $m = 0$
1	-9 ± 18 (†)	0 ± 4.4	0 ± 13	9.0 ± 6.2 (†)	$\|\|$ to feeds
	0 ± 22	0 ± 6.3	0 ± 13	0 ± 6.2	$\perp$ to feeds
	-9 ± 27	0 ± 7.1	0 ± 16	9.0 ± 9.5	Total $m = 1$
2	0 ± 1.4 (‡)	-8.8 ± 4.4	-5.6 ± 2.8	-5.1 ± 2.6	Detection inhomogeneity
	0 ± 3.2	0 ± 3.0	0 ± 2.2	0 ± 1.3	2 mm offset, homogeneous det.
	0 ± 3.5	-8.8 ± 5.3	-5.6 ± 3.5	-5.1 ± 2.9	Total $m = 2$
Total	-9.7 ± 27	-9.2 ± 8.9	-7.1 ± 16	3.7 ± 9.9	Total DCP

These corrections and uncertainties are given separately for each azimuthal term of the phase distribution, labeled with the azimuthal number m. The last row is the total DCP correction and uncertainty, given by the combination of $m = 0$, 1, and 2.

†For technical reasons not detailed here, FO1 and FO2-Rb are, to date, operating at a non-vanishing parallel effective tilt, hence the nonzero $m = 1$ correction.

‡The first $m = 2$ correction for FO1 is zero with a small uncertainty because of a $(45 \pm 5)^\circ$ angle between the feed axis and the detection axes.

TABLE II. CALCULATED MICROWAVE LENSING FRACTIONAL FREQUENCY SHIFTS FOR FO1, FO2, AND FOM, IN UNITS OF 10^{-17}.

	FO1	FO2-Cs	FOM	FO2-Rb
Analytic	7.8	8.4	11.9	7.0
Upward cavity aperture	6.1	7.0	9.2	5.8
All order dipole and upward cutoff aperture	5.7	6.5	8.6	5.6
Detection inhomogeneity and Ramsey contrast	6.5	7.3	9.0	6.8

The microwave lensing shift is given for each fountain with the approximations described in the text. From top to bottom, the degree of sophistication of the model is increasing. Our best final result is given in the last row.

C. Blackbody Radiation Shift

The blackbody radiation (BBR) shift is one of the largest systematic corrections and is a significant source of uncertainty in atomic fountains. The bulk of this shift is simply given by the scalar Stark shift of the clock transition [46], its response to a static electric field. A high-accuracy measurement of the Stark coefficient was made early on at LNE-SYRTE with FO1 [47] and subsequently used by most groups for their BBR corrections. These measurements were made with applied electric fields ranging from 50 to 150 kV·m^{-1}, significantly higher than the 831.9 V·m^{-1} rms value of the BBR field at 300K. The greatly improved measurement capability enabled by the CSO (see Section II-E) provides an opportunity to measure the Stark coefficient at an electric field strength that is much closer to a typical BBR field. The early measurements [47] were specifically tested for a possible deviation from a purely quadratic dependance on the electric field. This test did not show any such deviation, which was expected because there was no theoretical basis to expect significant higher-order terms given the measurement accuracy and field strengths. Nevertheless, it was important to re-examine these measurements at much lower fields given the intervening conflicting measurements and calculations of [48], [49], and [50].

These new measurements [51] at field strengths ranging from 1.5 to 25 kV·m^{-1} are in excellent agreement with the earlier measurements of [47]. To extract the scalar Stark coefficient for the BBR clock correction from these measurements, the small tensor contribution must be subtracted [47]. In [52], a sign error in the earlier theory [53], [54] for this tensor part was found, which was then confirmed experimentally [55]. Taking into account this revised theory, we get a corrected value for the scalar Stark coefficient: $k_0 = -2.282(4) \times 10^{-10}$ Hz·V^{-2}·m^2. The change in the BBR fractional frequency correction from the previous value of [47] is 6.8×10^{-17}, 80% of which is due to the sign correction of the theory. The uncertainty of k_0 continues to be dominated by the uncertainty on the geometry of the copper plates used to apply the electric field in the fountain. The value agrees with the most recent theoretical calculations [56]–[58]. It also agrees with several other calculations [46], [48], [59], [60], after some [48], [59] are corrected for omitted contributions pointed out in [56] and [57]. The only discrepancy that seems to remain, even after the omitted contributions are included, is the calculation in [52] (see [51, table summary]). We also note that a thermal atomic beam experiment recently provided another Stark shift coefficient measurement [61]. The still-preliminary value is in agreement with the LNE-SYRTE value and is ∼5 times less accurate.

We have also performed direct measurements of the BBR shift by inserting a blackbody tube in the FO1 fountain [62], exposing atoms to thermal radiation at temperatures ranging from 300K to 440K. Measurements were

in excellent agreement with the previously mentioned scalar Stark shift coefficient, but with a 22-times-larger uncertainty [51]. Ongoing comparisons between a room-temperature fountain and a cryogenic fountain [63] should yield another measurement of the Cs BBR shift at room temperature.

Regarding the BBR coefficient of the ^{87}Rb hyperfine frequency, the experimental status is unchanged from [64]. On the theoretical side, high-accuracy *ab initio* calculations have recently been published in [65] and [66].

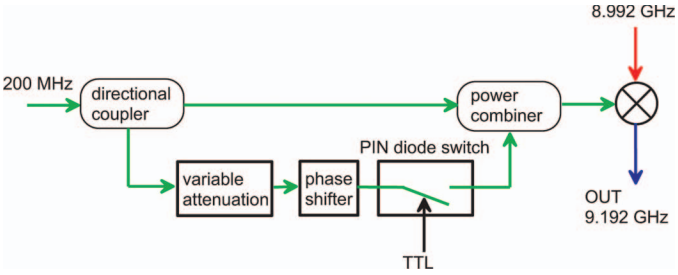

Fig. 7. Schematic of a switchable microwave synthesizer with a low phase transient using a Mach-Zehnder interferometric switch.

D. Microwave Leakage

In the last few years, we have developed a new approach to assess frequency shifts resulting from microwave leakage. Ideally, after the state-selection process, atoms interact with the interrogating microwaves only in the microwave cavity during the upward and downward traversals. In practice, unintended interactions can occur with a residual microwave field that is coherent with the probing field. Being unintended, such a residual field is by nature uncontrolled, with a potentially complex structure with both a large standing-wave and a large traveling-wave component. Such an extraneous field, which is difficult to exclude at the required level with purely electrical means, leads to a frequency shift which generally has a complicated variation with the fountain parameters, especially the microwave power [67], [68]. If present, the frequency shift is generally difficult to disentangle from other systematic errors such as the distributed cavity phase or the microwave lensing frequency shifts.

Our latest experimental approach to evaluate microwave leakage shifts uses microwave synthesizers, which not only will have intrinsically low microwave leakage but also can be switched off when the atoms are outside the microwave cavity. The challenge is to develop a switch that does not cause a large phase transient of the transmitted field after it is switched on. Fig. 7 depicts the architecture of our synthesizers. The interrogation signal at 9.192 GHz is generated by mixing a high-power 8.992-GHz signal with a small amount of 200-MHz signal to produce only the minimum needed power.

This architecture provides the ability to switch the carrier at the output by switching the 200-MHz signal. To minimize phase transients, the 200-MHz signal is switched using a Mach-Zehnder interferometric switch. The attenuator and the phase shifter are adjusted so that, when the PIN diode switch is closed, letting the signal pass through, destructive interference gives a dark fringe at the output of the interferometer. When the PIN diode switch is open, the on-state signal passes the direct channel of the interferometer with no component that is likely to produce a phase transient. Specifically, the phase transient occurring in the PIN diode as it is switched is circumvented.

The development of a heterodyne phase transient analyzer [10] was crucial to the successful implementation of switchable microwave synthesizers in Fig. 7 with low phase transients. This analyzer was used extensively to select components and identify the critical parameters to achieve the desired performance. Furthermore, this device can also be used to unveil spurious phase perturbations that are synchronous with the fountain cycle, with sensitivities as low as 1 μrad$\cdot$s^{-1} at the 9.192-GHz carrier frequency. Such perturbations can occur if some elements of the fountain sequence (switching of fairly high levels of RF power in acousto-optic modulators, switching of the state-selection microwave synthesizer, etc.) perturb the interrogation synthesizer through ground loops or other electromagnetic compatibility weaknesses. Required for the heterodyne phase transient analyzer, an independent reference synthesizer (the 6 to 9 GHz synthesis for other purposes shown in Fig. 4), is distributed through an actively compensated fiber link.

With a suitably characterized switchable synthesizer, it becomes possible to test for a putative microwave leakage by measuring the clock frequency with and without switched microwaves [10]. All of the LNE-SYRTE fountains (including FO2-Rb) are now equipped with a switchable synthesizer. Furthermore, the heterodyne phase transient analyzer is used to periodically search for synchronous perturbations.

E. Accuracy Budget

Our approach to dealing with other systematic shifts has been reported elsewhere and has not changed significantly since our last reviews [69] [70].

In FO1 and FO2-Cs, the large cold collision shift [4] is extrapolated to zero density in real time through interleaved measurements at a high density and a halved density. We use the interrupted adiabatic passage method [12], which gives accurate ratios of the atomic densities. Because of the much lower atom-number-dependent effects in ^{87}Rb [71]–[73], we change the atom number and density with the more conventional ways, either loading time or Rabi flopping in the state-selection cavity. It is also possible to adopt an approach in which a constant atom number is used most of the time, the collision shift being corrected based on a previously measured coefficient. The coefficient is measured with dedicated comparisons of high and low density, performed a few times per year. This approach is also used for FOM, which has a comparatively low cold collision shift because of a smaller atom number.

TABLE III. SYSTEMATIC FRACTIONAL FREQUENCY CORRECTIONS FOR FO1, FO2, AND FOM, IN UNITS OF 10^{-16}.

	FO1	FO2-Cs	FOM	FO2-Rb
Quadratic Zeeman shift	-1274.5 ± 0.4	-1915.9 ± 0.3	-305.6 ± 1.2	-3465.5 ± 0.7
Blackbody radiation	172.6 ± 0.6	168.0 ± 0.6	165.6 ± 0.6	122.8 ± 1.3
Collisions and cavity pulling	70.5 ± 1.4	112.0 ± 1.2	28.6 ± 5.0	2.0 ± 2.5
Distributed cavity phase shift	-1.0 ± 2.7	-0.9 ± 0.9	-0.7 ± 1.6	0.4 ± 1.0
Spectral purity and leakage	<1.0	<0.5	<4.0	<0.5
Ramsey and Rabi pulling	<1.0	<0.1	<0.1	<0.1
Microwave lensing	-0.7 ± 0.7	-0.7 ± 0.7	-0.9 ± 0.9	-0.7 ± 0.7
Second-order Doppler shift	<0.1	<0.1	<0.1	<0.1
Background collisions	<0.3	<1.0	<1.0	<1.0
Total	-1033.1 ± 3.5	-1637.5 ± 2.1	-113.0 ± 6.9	-3341.0 ± 3.3
Prior to 2011*	-1031.4 ± 4.1	-1635.9 ± 3.8	-111.4 ± 8.1	-3340.7 ± 4.2

The table gives the most recent values, taking into account the results of Tables I and II.
*The last row gives the overall corrections and uncertainties before 2011. Prior to 2011, the DCP correction was $(0.0 \pm 3.2) \times 10^{-16}$ for FO1, $(0.0 \pm 3.0) \times 10^{-16}$ for FO2-Cs, $(0.0 \pm 2.5) \times 10^{-16}$ for FO2-Rb. For FOM, the status of theory and experiment was such that the DCP effects and the effects related to spectral purity and leakage could not be disentangled, yielding a combined correction of $(0 \pm 6.0) \times 10^{-16}$. The microwave lensing correction was $(0.0 \pm 1.4) \times 10^{-16}$ for FO1, FO2-Cs, and FOM, and $(0.0 \pm 1.2) \times 10^{-16}$ for FO2-Rb.

Note that recently, another method has been proposed and demonstrated to deal with the cold collision shift of Cs [74], [75].

The accuracy budget for the LNE-SYRTE fountains is given in Table III. We give the most recent status, taking into account the latest evaluations of the distributed cavity phase shift and microwave lensing frequency shifts as reported in Table I and II. In the absence of an independent calculation or experimental investigation, the uncertainty for the microwave lensing is conservatively taken to be equal to the calculated value. The last row of Table III gives the status of the accuracy budgets before 2011.

IV. APPLICATIONS IN TIME AND FREQUENCY METROLOGY

A. ^{133}Cs Fountain Comparisons

For more than a decade, the development of LNE-SYRTE fountain ensemble of Fig. 4 has allowed high-accuracy comparisons between atomic fountain clocks. This has especially been the case in the last few years, during which hundreds of days of clock comparisons have accumulated.

To deal with the differences in clock cycles, mode of operation, schedule for verifying the magnetic field, etc., we apply the following data-processing scheme. Each fountain produces measurements, corrected for all systematic biases, at a rate of 1 measurement per cycle. When an interleaved sequence of high and low density measurements is used, this first step requires the use of these interleaved data to determine the cold collision shift coefficient for a particular time window, and then to correct the high- and low-density frequency measurements accordingly.

The individual fountain measurements are averaged over time intervals of 864 s (1/100th of a day) starting at the beginning of the day. Intervals are discarded if the number of valid fountain cycles is below a chosen threshold, for instance, because of an automated verification of the magnetic field, a laser going out of lock, or a phase/frequency jump in the output of the cryogenic oscillator. Other filters can be applied based on fault of the CSO, one of the fiber links, or other subsystems. This leaves a set of validated data in which the sampling sequence is matched between all fountains. These data represent measurements by each fountain of the frequency of the common ultra-stable reference, i.e., the 11.98-GHz signal weakly phase-locked to one of the hydrogen masers (see Fig. 4), which are used for calibration of the international atomic time (see Section IV-C).

As a third step, the frequency difference between the synchronous validated data of two fountains eliminates the frequency of the common-mode ultra-stable reference and allows a direct comparison. An example of frequency instability between FOM and FO2 over 50 effective days of averaging is shown in Fig. 8. Here, the overall short-term instability is $1.3 \times 10^{-13}\tau^{-1/2}$ and the measurement resolution is ~2 parts in 10^{16} after averaging for 4.5 days. The best reported instability for this type of comparison is $5.0 \times 10^{-14}\tau^{-1/2}$ [9], [69], [70].

Fountain comparisons following this data-processing scheme are now performed regularly at LNE-SYRTE. It was recently incorporated into a fully automated procedure. In addition to daily updates of the fountain comparisons, an overview of the systems' parameters is generated to help assess the status of the clock ensemble in quasi-real-time with hourly updates. To produce fully validated data for fountain comparisons, for example, for timescale steering and TAI calibrations, the entire data processing is critically scrutinized and redone if necessary. Fig. 9 shows the monthly average of fractional frequency differences D between the three Cs fountain pairs from November 2006 to April 2011. These data correspond to a

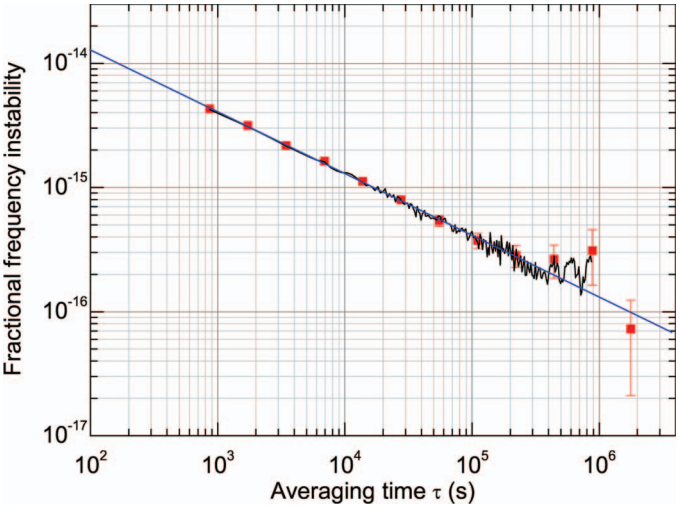

Fig. 8. Fractional frequency instability between the FO2 and FOM Cs fountains as a function of the averaging time τ. The data correspond to 50 effective days of comparisons between MJD 55551 and MJD 55663. Red points with error bars give the instability at $\tau = 2^N \times 864$ s. The black curve shows the instability for all τ.

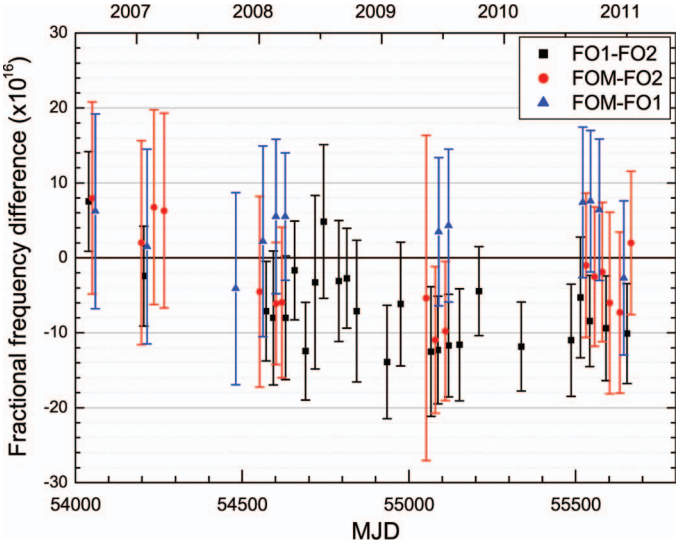

Fig. 9. Fractional frequency differences between the three pairs of LNE-SYRTE Cs fountains from Nov. 2006 to Apr. 2011. Error bars are the total uncertainties, which are dominated by systematic uncertainties.

TABLE IV. SUMMARY OF CS FOUNTAIN COMPARISONS OVER THE NOVEMBER 2006 TO APRIL 2011 PERIOD.

	Duration (d)	D	U	$\lvert D/U\rvert$	χ^2_{D}	Q_{D}	χ^2_0	Q_0
FOM–FO2	320	−3.0	9.1	0.33	0.28	0.996	0.37	0.983
FOM–FO1	240	4.1	9.2	0.44	0.12	0.999	0.28	0.989
FO1–FO2	500	−5.7	6.2	0.92	1.48	0.55	2.12	0.001

The first column gives the accumulated number of days of comparison. D is the fractional frequency difference and U the overall uncertainty, both in units of 10^{-16}. χ^2_{D} is the reduced χ^2 with respect to the mean difference D. χ^2_0 is the reduced χ^2 with respect to the expected null difference. Q_{D} and Q_0 are the corresponding goodness-of-fit as defined in [76].

total of ∼1000 effective days of fountain comparison. The error bars are the total uncertainties for a given clock pair, which are dominated by the systematic uncertainties of the two fountains. The overall fractional frequency differences D (weighted averages) are reported in Table IV, together with the corresponding overall uncertainties U. $|D/U|$ represents the deviation from a null difference scaled to the 1σ total uncertainty. The reduced χ^2, either with respect to the mean (χ^2_{D}) or with respect to zero (χ^2_0) gives a further consistency check of these data. Finally, the goodness-of-fit[3], as defined in [76], can be computed, either with respect to the mean (Q_{D}) or with respect to zero (Q_0). The Qs very close to 1 for FOM-FO2 and FOM-FO1 indicate that fluctuations about the means are smaller than the total uncertainties. Q_0 which tests deviations (and/or fluctuations) from the expected null difference shows that FOM–FO2 and FOM–FO1 agree within the total uncertainties. However, the low Q_{D} and Q_0 for the more stringent FO1–FO2 comparison indicates a slightly underestimated systematic effect, of a few 10^{-16}, which is under investigation. Note that for the data of Fig. 9, the modifications from our recent study of the DCP shift (see Section III-A and [39]) were not yet implemented. Consequently, the DCP shift is one potential candidate to explain these deviations. Future comparisons, after a full implementation to all fountains of the modified approach to the DCP shift, will clarify this point.

Note that a somewhat similar analysis of worldwide comparisons of fountain primary frequency standards exploiting their calibrations of TAI is reported in [77].

B. A Secondary Representation of the SI Second

Following the early demonstration of the low cold collision shift in ^{87}Rb [71], [72], LNE-SYRTE has performed a series of high-accuracy absolute measurements of the ^{87}Rb hyperfine frequency against Cs fountain clocks [3], [64], [78]. The 2003 comparison was the most accurate of any atomic frequency comparison at the time. Since then, it has been superseded by rapidly improving optical frequency measurements. The ^{87}Rb hyperfine frequency was the first secondary representation of the SI second recognized by BIPM [79]. Its recommended value is given by the 2002 LNE-SYRTE measurement: 6 834 682 610.904324 Hz

[3]The goodness-of-fit Q is the probability that a value of chi-squared as poor as the value found with the data should occur by chance. Quoting [76]: "If Q is larger than, say, 0.1, then the goodness-of-fit is believable."

with a recommended uncertainty of 21 μHz, or 3 parts in 10^{15}. This recommended uncertainty was chosen to be ~3 times larger than the actual uncertainty of the measurement (1.3×10^{-15}). Our latest reported measurement (4 μHz uncertainty, or 5.9 parts in 10^{16}), together with an analysis of the consistency of all our measurements, can be found in [3]. An independent ^{87}Rb versus ^{133}Cs fountain comparison was reported for the first time in 2010. Agreement with LNE-SYRTE measurements is claimed at the 10^{-15} level, but the actual result of the measurement has not yet been reported [80]–[82]. Also notable is the construction of at least 8 Rb fountains at the US Naval Observatory [83], [84].

C. Contributions to TAI

Since 2007, LNE-SYRTE fountains have measured the frequency of one of LNE-SYRTE H-masers almost continuously. These data are used to calibrate TAI. Fig. 10 shows all calibrations of TAI by LNE-SYRTE cesium fountains since November 2004. Each data point corresponds to a measurement, by one fountain, of the H-maser average frequency over a 20- to 30-day period, reaching a typical statistical uncertainty of 3×10^{-16}, which is augmented in quadrature by an uncertainty resulting from dead times of, typically, 1.5×10^{-16}. (See *Circular T* and fountain reports on the BIPM website: http://www.bipm.org/jsp/en/TimeFtp.jsp.) Between the 2007 and 2010 period, LNE-SYRTE reported 78 formal evaluations to BIPM, out of a total of 161 fountain reports worldwide, i.e., LNE-SYRTE has contributed almost 50% of all reports since 2007. For contributions to TAI, the gravitational redshift corrections are -69.3×10^{-16}, -65.4×10^{-16}, and -68.7×10^{-16}, for FO1, FO2, and FOM respectively, with an uncertainty of 1.0×10^{-16} corresponding to a 1-m uncertainty of height above the geoid. Contributions to TAI also provide a vehicle to compare with other fountain clocks around the world. The latest update on these comparisons appears in [77].

Since mid-2006, fountain data, including from FO2-Rb, have been used to steer the French Atomic Time [TA(F)] on a monthly basis. TA(F) is a timescale based on an ensemble of commercial Cs clocks located in France and elaborated at LNE-SYRTE. This steering has improved the long-term stability of the timescale with respect to TAI [85].

D. Absolute Measurements of Optical Frequencies

The accuracy and stability of optical atomic clocks have now largely surpassed those of microwave clocks, and notably atomic fountain clocks [86]–[89]. This opens a path to redefining the SI second using an optical transition [90]. One of the prerequisites to a redefinition is absolute frequency measurements of potential optical transitions with the highest accuracy. The LNE-SYRTE fountain clock ensemble (Fig. 4) offers some unique features to contribute

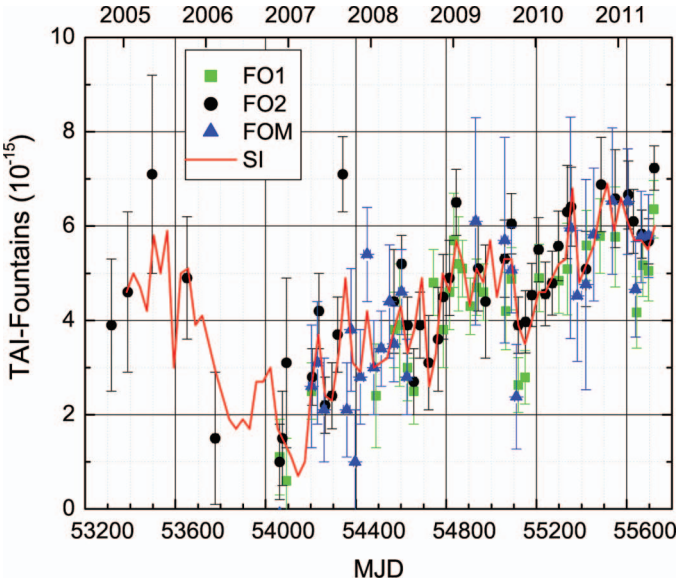

Fig. 10. Calibrations of the International Atomic Time (TAI) by the LNE-SYRTE fountains since 2004. The data are from BIPM *Circular T*. Each point is the fractional frequency difference between TAI and the SI second as measured by one of LNE-SYRTE's fountains, and corresponds to a formal monthly report to BIPM. The red curve is the difference between TAI and the SI second, as computed by BIPM from all available primary standards.

to this task. This includes the availability of several fountains for redundant measurements, of an ultra-low-noise reference signal that provides the best reported stability to date between a microwave and optical clock [91], and of the transportable fountain FOM for measuring optical frequency at other laboratories. Absolute frequency measurements of optical frequencies can also probe the stability of fundamental constants [92]–[95], determine the Rydberg constant [96], and test quantum electrodynamics (QED) [97].

Next, we give an overview of absolute optical frequency measurements made with the LNE-SYRTE fountain ensemble.

1) Hydrogen 1S–2S Transition Measured With FOM at MPQ, Garching, Germany: At the Max Planck Institut für Quantenoptik (MPQ) in Garching, Germany, we have measured the absolute frequency of the 1S–2S optical transition via 2-photon excitation at 246 nm [93], [98], [99]. Three measurement campaigns were completed in 1999, 2003, and 2010. For these experiments, a femto-comb laser is used to measure the frequency of the excitation laser. The repetition rate is locked to a hydrogen maser whose frequency is simultaneously measured directly by FOM. The noise of the maser signal is filtered by phase-locking a BVA quartz oscillator to improve the measurement stability. The last measurement in 2010 had the best fractional uncertainty: 4.2×10^{-15} [99]. The measured 1S–2S transition frequency is 2 466 061 413 187 035 (10) Hz.

High-resolution spectroscopy of hydrogen is interesting to test highly accurate atomic structure calculations for

QED tests [100]. Also, the recent capture of antihydrogen at CERN [101] is a first step toward cooling of antimatter to enable high-resolution spectroscopy of antihydrogen for fundamental tests of charge, parity, time-reversal (CPT) symmetry and the gravity of antimatter.

2) $^{40}Ca^{+}$ Optical Clock Measured With FOM at the University of Innsbruck, Austria: In 2007, at the Institut für Experimentalphysik and Quantenoptik, University of Innsbruck, Austria, we measured the absolute frequency of the 4s $^2S_{1/2}$−3d $^2D_{5/2}$ optical quadrupole transition of a trapped single $^{40}Ca^{+}$ ion. The frequency of this transition is 411 042 129 776 393.2 (1.0) Hz [102]. This corresponds to a fractional frequency uncertainty of 2.4 parts in 10^{15}. During this experiment, FOM was used in the autonomous configuration mentioned in Section II-D, in which a BVA quartz oscillator is frequency locked to the FOM spectroscopic signal. The output of the BVA quartz oscillator synchronizes the repetition rate of the femtocomb laser that measures the probe laser frequency for the $^{40}Ca^{+}$ transition. This quadrupole transition in a $^{40}Ca^{+}$ ion is another candidate for an optical clock and for tests of the stability of fundamental constants.

3) ^{88}Sr and ^{88}Sr Optical Lattice Clocks Measured at SYRTE: LNE-SYRTE is developing two Sr optical lattice clocks. During their development, several absolute frequency measurements of the Sr clock frequency were made [91], [103]–[105]. The best reported uncertainty for these measurements is 2.6×10^{-15} [91]. Both titanium:sapphire-based and Er-doped fiber-based optical frequency combs were used to measure the frequency of the 698-nm laser light stabilized to the Sr atoms. The 2006 measurements of ^{87}Sr used a fiber optical frequency comb transported from the Physikalisch Technische Bundesanstalt (PTB) in Braunschweig, Germany [91], [104]. As previously mentioned, the ultra-stable reference based on a CSO (Fig. 4) allows the best short-term stability reported to date for comparing an optical clock to a microwave clock: $6 \times 10^{-14}\tau^{-1/2}$. In the recent measurements, the optical frequency comb is stabilized to an ultra-stable laser as described in [22], making the repetition rate of the femtosecond laser an ultra-stable microwave signal. This signal is then measured against the CSO-based ultra-stable reference, which is in turn measured by the fountain clocks. Simultaneously, the beat between the optical frequency comb and the 698-nm light is counted to extract its absolute frequency. The stability of fundamental constants is stringently tested by combining these with similar measurements by other institutes [92].

4) Measurement of ^{199}Hg and ^{201}Hg Optical Clock Transition Frequencies at SYRTE: LNE-SYRTE is developing an optical lattice clock based on neutral mercury. The first absolute frequency measurements of the ^{199}Hg and ^{201}Hg optical clock transition were in 2008 [106]. These initial measurements improved the previous knowledge of the transition frequency by more than 4 orders of magnitude, to a fractional frequency uncertainty of 5×10^{-12}. More recently, measurements against LNE-SYRTE ultra-stable reference were used to perform the first experimental determination of the magic wavelength for Hg [107]. Ongoing development of the Hg clock is expected to soon yield measurements at the 10^{-15} level and beyond.

E. Other Measurements With the Transportable Fountain FOM

We have performed frequency comparisons with the engineering model of the space clock PHARAO (see Section VI and [108]) between 2007 to 2009, at the Centre National d'Etudes Spatiales (CNES) in Toulouse, France. We have also verified the frequency performance of the ACES architecture [109]. The test included a ground model of the onboard data handling unit (XPLC), the frequency comparison and distribution package (FCDP), the PHARAO engineering model, and a ground model of the space hydrogen maser (SHM). The two clocks are combined to generate a timescale with the short-term stability of SHM and the long-term stability and accuracy of PHARAO.

F. Remote Comparisons via T2L2 Satellite Laser Link

In 2010, time transfer by the T2L2 laser link via the JASON2 satellite [110] was tested by comparing FOM at the Observatoire de la Côte d'Azur (OCA) in Grasse, France, with the other LNE-SYRTE fountains at the Observatoire de Paris. The common time transfer techniques, carrier-phase GPS and TWSTFT, were also used in parallel. Notable in this comparison is the large gravitational redshift, -1.384×10^{-13}, at the OCA altitude of 1268 m. Preliminary results [111] show that all the time transfer methods are consistent to within 2 ns over 2 months. The frequency difference between the remote fountains is measured with a typical uncertainty of 1×10^{-15}, which determines the gravitational redshift difference to 10^{-2}. It now remains to refine the analysis and to evaluate the ultimate performances of the T2L2 time transfer link. Note that at MPQ, at CNES, and at OCA, FOM also provided calibration of the TAI by using a GPS receiver and a carrier-phase GPS analysis software developed by CNES or by NRCAN. This is the first time that a primary frequency standard contributes to steering the TAI from different sites with different gravitational redshifts [112].

V. Applications in Fundamental Physics

One of the most interesting applications of atomic clocks is to test fundamental physics. In this section, we review contributions of LNE-SYRTE fountain ensemble to such tests.

A. Stability of Constants

Repeated high-accuracy comparisons between atomic (or molecular) frequencies can test the stability of fun-

damental constants such as the fine structure constant α or the electron to proton mass ratio m_e/m_p (see, for instance [113], [114], and references therein). Laboratory experiments usefully complement tests over cosmological timescales because the interpretation does not rely on any assumptions about a cosmological model [115], [116].

A first test performed with the LNE-SYRTE fountain ensemble comes from a series of ^{87}Rb versus ^{133}Cs hyperfine frequency comparisons made during the development of the FO2 dual Rb/Cs fountain [69], [70], [78], and [117]. In this last 2008 report, a putative time variation of the ratio of the two hyperfine frequencies is constrained to $d\ln(\nu_{Rb}/\nu_{Cs})/dt = (-3.2 \pm 2.3) \times 10^{-16}\ \mathrm{yr}^{-1}$. In terms of fundamental constants, this result yields $d\ln(\alpha^{-0.49}[g_{Rb}/g_{Cs}])/dt = (-3.2 \pm 2.3) \times 10^{-16}\ \mathrm{yr}^{-1}$, where g_{Rb} and g_{Cs} are the nuclear g-factors in ^{87}Rb and ^{133}Cs. Expressing these g-factors in terms of fundamental parameters of the standard model [118], [119] gives: $d\ln(\alpha^{-0.49}[m_q/\Lambda_{QCD}]^{-0.025})/dt = (-3.2 \pm 2.3) \times 10^{-16}\ \mathrm{yr}^{-1}$, where Λ_{QCD} is the mass scale of quantum chromodynamics (QCD). An improved analysis including more recent measurements, with FO2 in the dual fountain configuration, will improve this value significantly.

A second test comes from a series of absolute frequency measurements of the ^{87}Sr optical lattice clock by LNE-SYRTE (see Section IV-D-3), the University of Tokyo, Japan, and JILA, Boulder, CO [92]. Together, these constrain the putative variation of ν_{Sr}/ν_{Cs} to $d\ln(\nu_{Sr}/\nu_{Cs})/dt = (-7 \pm 18) \times 10^{-16}\ \mathrm{yr}^{-1}$, corresponding to $d\ln(\alpha^{2.77}[m_q/\Lambda_{QCD}]^{-0.039}[m_e/\Lambda_{QCD}])/dt = (-7 \pm 18) \times 10^{-16}\ \mathrm{yr}^{-1}$. The same measurements constrain the putative variation of this same combination of constants with the gravitational potential to $c^2 d\ln(\alpha^{2.77}[m_q/\Lambda_{QCD}]^{-0.039}[m_e/\Lambda_{QCD}])/dU = (-5.8 \pm 8.9) \times 10^{-6}$, where c is the speed of light and U is the gravitational potential[4]. This test relies on exploiting the yearly modulation of the gravitational potential of the Sun due to the eccentricity of the Earth's orbit.

Measurements of the H(1S–2S) transition performed at MPQ Garching (see Section IV-D-1) using the transportable fountain FOM as a reference, offer a third test: $d\ln(\nu_{H(1S-2S)}/\nu_{Cs})/dt = (-3.2 \pm 6.3) \times 10^{-15}\ \mathrm{yr}^{-1}$ [93]. This translates to $d\ln(\alpha^{2.83}[m_q/\Lambda_{QCD}]^{-0.039}[m_e/\Lambda_{QCD}])/dt = (-3.2 \pm 6.3) \times 10^{-15}\ \mathrm{yr}^{-1}$, a constraint which will soon improve as a result of a recent measurement campaign [99].

A fourth test comes from a series of comparisons between the ^{133}Cs and the hydrogen hyperfine frequencies. LNE-SYRTE fountain's contributions to this test were the calibrations of TAI reported in BIPM *Circular T* (see Section IV-C) enabling the connection with 4 hydrogen masers participating to the elaboration of the NIST AT1 atomic timescale (see, for instance, [120]). Other Cs fountain contributions to the experiment came from PTB in Germany and from the Istituto Nazionale di Ricerca Metrologica (INRIM) in Italy. The analysis was performed at the National Institute of Standards and Technology (NIST), Boulder, CO [121] and gives $|c^2 d\ln(\nu_H/\nu_{Cs})/dU| = (0.1 \pm 1.4) \times 10^{-6}$, corresponding to $|c^2 d\ln(\alpha^{0.83}[m_q/\Lambda_{QCD}]^{0.11})/dU| = (0.1 \pm 1.4) \times 10^{-6}$.

Note that instead of using α, m_q/Λ_{QCD}, and m_e/Λ_{QCD} as independent variables, α, $\mu = m_e/m_p$, and m_q/m_p can be used. The link between the two approaches is $d\ln(m_p/\Lambda_{QCD}) \simeq 0.048 \times d\ln(m_q/\Lambda_{QCD})$ [119].

B. Test of Lorentz Invariance in the Matter Sector

The LNE-SYRTE FO2 fountain has tested the anisotropy of space as in Hughes-Drever experiments (see, for instance, [122]). For this experiment, the fountain sequence is tailored to probe opposing Zeeman transitions in ^{133}Cs to test for a putative variation of their frequencies when the orientation of the quantization axis changes (here, because of the Earth's rotation) with respect to a supposedly preferred frame [123], such as the frame of the cosmic microwave background. The experiment was interpreted within the framework of the Lorentz-violating standard model extension (SME), where it is sensitive to proton parameters corresponding to a largely unexplored region of the SME parameter space. The constraints for 4 parameters, already constrained by other measurements, were improved by as much as 13 orders of magnitude and 4 parameters were constrained for the first time. Operating FO2 in the dual Rb/Cs configuration [3] opens new possibilities for improving and complementing these tests.

C. Other Tests

The development of the LNE-SYRTE fountain ensemble also offered a test of Lorentz local invariance in the photon sector, not using the fountains, but simply by comparing the CSO to a hydrogen maser (see Fig. 4) for a duration that now exceeds 10 years. This experiment is, to date, the most stringent Kennedy-Thorndike test by a factor of 500. The latest update is published in [124]. The experiment can also be interpreted in the SME framework [125].

VI. Development of the PHARAO Cold Atom Space Clock

Atomic Clocks Ensemble in Space (ACES) is a European Space Agency (ESA) fundamental physics mission originally proposed by Laboratoire Kastler Brossel and SYRTE. It is based on the operation of highly stable and accurate atomic clocks in the microgravity environment of the International Space Station (ISS) [109]. The time scale generated by the ACES clocks on-board the ISS is delivered to Earth through a high-performance two-way time and frequency transfer link. The clock signal is used to perform space-to-ground as well as ground-to-ground

[4]For instance, the gravitational potential created by a point mass m at a distance r is: $U(r) = Gm/r$, where G is the Newtonian constant of gravitation.

comparisons of atomic frequency standards. The ACES scientific objectives cover both fundamental physics and applications. Tests of special and general relativity will be performed with improved accuracy, as well as a search for temporal variations of fundamental constants. On the application side, frequency comparisons between distant clocks, both space-to-ground and ground-to-ground, will be performed worldwide with unprecedented resolution. ACES will demonstrate a new type of relativistic geodesy, which, based on a precision measurement of the Einstein's gravitational redshift, will resolve differences in the Earth's gravitational potential at the 10-cm level. Finally, ACES will contribute to the improvement of global navigation satellite systems (GNSS) and to future evolutions of these systems. It will demonstrate new methods to monitor the ocean surface based on scatterometric measurements of the GNSS signal and it will contribute to the monitoring of the Earth's atmosphere through radio-occultation experiments. The expected performance is a time stability of 10 ps over 10 days (1 ps for common-view comparisons between ground clocks) and a frequency accuracy better than 3×10^{-16}. The accuracy and the long-term frequency stability are defined by the PHARAO clock, an instrument developed by the French space agency CNES and SYRTE. The clock uses cold cesium atoms, slowly moving through a Ramsey cavity. We have fully tested the engineering model (PHARAO-EM) of the clock [108]. Fig. 11 shows a picture of the PHARAO-EM under test at the CNES assembly room in Toulouse. For nominal operation, the frequency stability is $3.3 \times 10^{-13}\tau^{-1/2}$. The central Ramsey resonance linewidth is 5.6 Hz and 10^6 atoms are detected. The contrast is only 93% (Fig. 12) because, on Earth, the atoms do not spend the same time in the two interaction zones of the Ramsey cavity.

On Earth, the clock cycle duration lasts 790 ms with a microwave interrogation time of 90 ms. Consequently the phase noise of the microwave signal, synthesized from a quartz oscillator, contributes to the frequency instability at a level of $2.2 \times 10^{-13}\tau^{-1/2}$. We have performed an accuracy evaluation of the clock. The main frequency corrections and their uncertainties are shown in Table V. The total frequency uncertainty is 1.9×10^{-15}. The largest uncertainty is the quadratic Zeeman shift because the magnetic field along the atomic trajectories is not homogeneous due to a problem with the innermost magnetic shield. The second largest contribution is the cold collision frequency shift. The frequency shift per detected atom is similar to other cold cesium clocks and the uncertainty is mainly limited by the measurement duration (only two weeks). The blackbody radiation shift is deduced from measurements of the ambient temperature. A technical problem prevented us from using the calibrated temperature probes located next to the Ramsey cavity. Finally, the first-order Doppler frequency shift has a large value because the atom's axial velocity decreases because of the gravity field, which causes the longitudinal DCP shifts from the 2 interactions to not cancel. This gives a large DCP shift that has a large dependance on the microwave field amplitude.

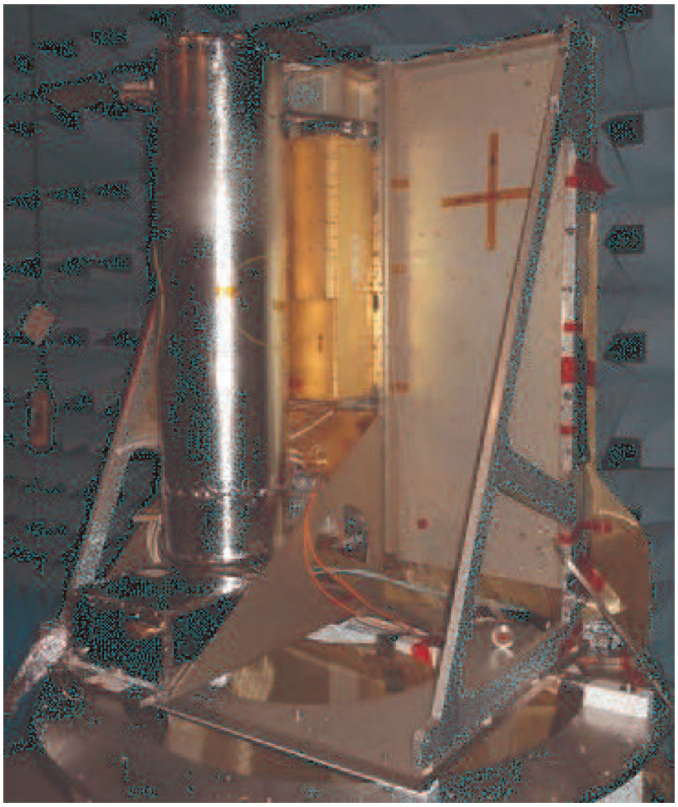

Fig. 11. The engineering model of the PHARAO cold atom space clock under test at CNES, Toulouse (photo is courtesy of CNES). The picture shows the vertically mounted cesium tube, the vacuum chamber surrounded by the magnetic shields. The gold-coated box behind the cesium tube contains the laser source. A second gold-coated box, below the laser source, is the microwave synthesizer. The black box in front, at the bottom of the cesium tube, is the on-board computer unit.

The PHARAO-EM clock, operated in several configurations, was compared with the transportable fountain FOM. After applying all systematic corrections (Tables III and V), the frequency differences were smaller than 2×10^{-15}, with a resolution of 5×10^{-16}. During these measurements, the accuracies of the clocks were 8.1×10^{-16} for FOM and 1.9×10^{-15} for PHARAO-EM. Consequently, there is no significant frequency offset between the clocks. Testing the engineering model demonstrated the full operation of the PHARAO clock architecture and highlighted some improvements to implement in the flight model. The PHARAO flight model is now being assembled and it will be delivered in 2012, together with the other ACES instruments. The launch date will be 2 years after the delivery of all of the instruments.

SYRTE will be a master station to survey and to analyze the ACES signal. One of the microwave link stations developed for ACES will be installed on the roof of a building at the Observatoire de Paris. Hydrogen masers steered by the atomic fountains and UTC(OP) will synchronize the station, forming the ACES ground segment at SYRTE. Strontium and mercury optical lattice clocks

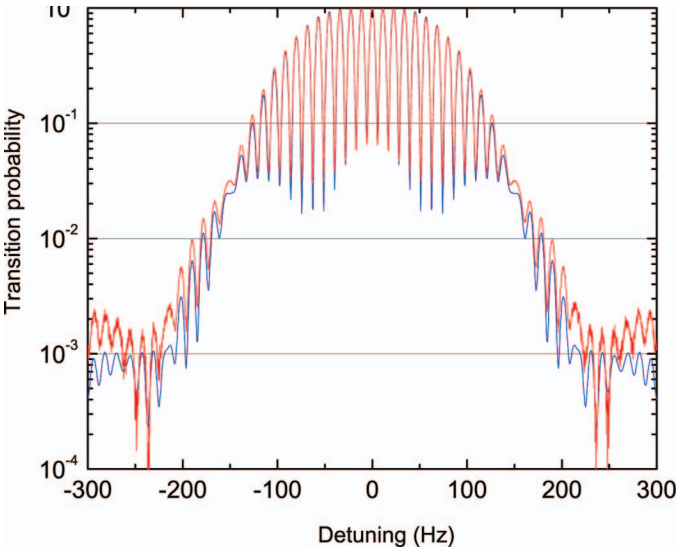

Fig. 12. Experimental (red) and calculated (blue) Ramsey fringes of the PHARAO-EM tested on Earth. The central fringe does not have the highest contrast because, operating on Earth, gravity leads to different interaction times on the two cavity interactions.

TABLE V. SYSTEMATIC FRACTIONAL FREQUENCY CORRECTIONS FOR THE PHARAO ENGINEERING MODEL DURING THE 2009 TESTS, IN UNITS OF 10^{-16}.

	Correction	Uncertainty
Quadratic Zeeman effect	−5633	14
Blackbody radiation	162.5	2.2
Cold collisions and cavity pulling	63	11
First-order Doppler	−33	5
Total	−5440	19

at SYRTE [107], [126], which are connected to the fountain ensemble via optical frequency combs, will also contribute to the ACES mission. Notably, ACES will provide ground-to-ground comparisons of these optical clocks to similar clocks at other institutes around the world, demonstrating relativistic geodesy.

VII. CONCLUSIONS

This paper gives an extensive overview of the development of the LNE-SYRTE fountain ensemble. We can also identify some priorities for the future. For fountains, it will be important to further improve inter-comparisons to reduce inaccuracies to 1 to 2 parts in 10^{16}, and to possibly remove yet unidentified sources of uncertainty or instability. Implementing more sophisticated microwave cavity designs is one interesting approach. Simultaneously, the reliability of the fountain ensemble must further improve. This is required by the ground segment of the ACES mission—quasi-continuous operation at the best accuracy of the three fountains for at least 18 months. This will be achieved by several technical improvements in the fountains (notably the laser systems), the fountain environment, and by complementing the cryogenic sapphire oscillator with a second low-noise microwave source derived from an ultra-stable laser. This system will also ensure a permanent link to the optical clocks. Achieving these goals will enable new or improved applications: realization of an ultra-stable local timescale, continuously steered to the atomic fountains; even more regular calibrations of TAI; improved measurements of optical frequencies; enhanced tests of fundamental physics; measurement of the gravitational redshift within the ACES project; and remote clock comparisons via ACES.

ACKNOWLEDGMENTS

Systèmes de Référence Temps-Espace (SYRTE) is UMR CNRS 8630 between Centre National de la Recherche Scientifique (CNRS), Université Pierre et Marie Curie (UPMC), and Observatoire de Paris. Laboratoire National de Métrologie et d'Essais (LNE) is the French National Metrology Institute. SYRTE is a member of Institut Francilien de Recherche sur les Atomes Froids (IFRAF) and of the C'Nano network of the Région Île de France. K. Gibble acknowledges support from the NSF, Penn State, and la Ville de Paris. We acknowledge a tremendous number of past contributions over 2 decades of development of the LNE-SYRTE fountain ensemble. We specifically acknowledge the contribution of SYRTE technical services. The ACES mission is an ESA project. Within ACES, the PHARAO cold atom space clock is developed and funded by CNES. The transportable fountain FOM is also funded by CNES to a large extent.

REFERENCES

[1] A. Clairon, P. Laurent, G. Santarelli, S. Ghezali, S. Lea, and M. Bahoura, "A cesium fountain frequency standard: Recent results," *IEEE Trans. Instrum. Meas.*, vol. 44, no. 2, pp. 128–131, 1995.

[2] P. Laurent, P. Lemonde, E. Simon, G. Santarelli, A. Clairon, N. Dimarcq, P. Petit, C. Audoin, and C. Salomon, "A cold atom clock in absence of gravity," *Eur. Phys. J. D*, vol. 3, pp. 201–204, 1998.

[3] J. Guéna, P. Rosenbusch, P. Laurent, M. Abgrall, D. Rovera, G. Santarelli, M. Tobar, S. Bize, and A. Clairon, "Demonstration of a dual alkali Rb/Cs fountain clock," *IEEE Trans. Ultrason. Ferroelectr. Freq. Control*, vol. 57, no. 3, pp. 647–653, 2010.

[4] K. Gibble and S. Chu, "A laser cooled Cs frequency standard and a measurement of the frequency shift due to ultra-cold collisions," *Phys. Rev. Lett.*, vol. 70, no. 12, pp. 1771–1774, 1993.

[5] X. Baillard, A. Gauguet, S. Bize, P. Lemonde, P. Laurent, A. Clairon, and P. Rosenbusch, "Interference-filter-stabilized external-cavity diode lasers," *Opt. Commun.*, vol. 266, no. 2, pp. 609–613, 2006.

[6] A. Clairon, C. Salomon, S. Guellati, and W. Phillips, "Ramsey resonance in a Zacharias fountain," *Europhys. Lett.*, vol. 16, no. 2, pp. 165–170, 1991.

[7] D. Chambon, M. Lours, F. Chapelet, S. Bize, M. E. Tobar, A. Clairon, and G. Santarelli, "Design and metrological features of microwave synthesizers for atomic fountain frequency standard," *IEEE Trans. Ultrason. Ferroelectr. Freq. Control*, vol. 54, no. 4, pp. 729–735, 2007.

[8] G. Santarelli, P. Laurent, P. Lemonde, A. Clairon, A. G. Mann, S. Chang, A. N. Luiten, and C. Salomon, "Quantum projection noise

in an atomic fountain: A high stability cesium frequency standard," *Phys. Rev. Lett.*, vol. 82, no. 23, pp. 4619–4622, 1999.

[9] C. Vian, P. Rosenbusch, H. Marion, S. Bize, L. Cacciapuoti, S. Zhang, M. Abgrall, D. Chambon, I. Maksimovic, P. Laurent, G. Santarelli, A. Clairon, A. Luiten, M. Tobar, and C. Salomon, "BNM-SYRTE fountains: Recent results," *IEEE Trans. Instrum. Meas.*, vol. 54, no. 2, pp. 833–836, 2005.

[10] G. Santarelli, G. Governatori, D. Chambon, M. Lours, P. Rosenbusch, J. Guéna, F. Chapelet, S. Bize, M. Tobar, P. Laurent, T. Potier, and A. Clairon, "Switching atomic fountain clock microwave interrogation signal and high-resolution phase measurements," *IEEE Trans. Ultrason. Ferroelectr. Freq. Control*, vol. 56, no. 7, pp. 1319–1326, Jul. 2009.

[11] K. Dieckmann, R. J. C. Spreeuw, M. Weidemüller, and J. T. M. Walraven, "Two-dimensional magneto-optical trap as a source of slow atoms," *Phys. Rev. A*, vol. 58, no. 5, pp. 3891–3895, Nov. 1998.

[12] F. Pereira Dos Santos, H. Marion, S. Bize, Y. Sortais, A. Clairon, and C. Salomon, "Controlling the cold collision shift in high precision atomic interferometry," *Phys. Rev. Lett.*, vol. 89, no. 23, art. no. 233004, 2002.

[13] F. Chapelet, "Fontaine atomique double de Césium et de Rubidium avec une exactitude de quelques 10^{-16} et applications," Ph.D. dissertation, Physics Dept., Université de Paris XI, Orsay, France, 2008, (in French).

[14] Y. Sortais, "Construction d'une fontaine double à atomes froids de ^{87}Rb et de ^{133}Cs, étude des effets dépendant du nombre d'atomes dans une fontaine," Ph.D. dissertation, Physics Dept., Université de Paris VI, Paris, France, 2001, (in French).

[15] S. Bize, "Tests fondamentaux à l'aide d'horloges à atomes froids de rubidium et de cesium," Ph.D. dissertation, Physics Dept., Université de Paris VI, Paris, France, 2001, (in French).

[16] R. Legere and K. Gibble, "Quantum scattering in a juggling atomic fountain," *Phys. Rev. Lett.* [Online]. vol. 81, no. 26, pp. 5780–5783, 1998. Available: http://link.aps.org/doi/10.1103/PhysRevLett.81.5780

[17] R. A. Hart, X. Xu, R. Legere, and K. Gibble, "A quantum scattering interferometer," *Nature* [Online]. vol. 446, no. 7138, pp. 892–895, Apr. 2007. Available: http://dx.doi.org/10.1038/nature05680

[18] F. Allard, I. Maksimovic, M. Abgrall, and P. Laurent, "Automatic system to control the operation of an extended cavity diode laser," *Rev. Sci. Instrum.* [Online]. vol. 75, no. 1, pp. 54–58, 2004. Available: http://link.aip.org/link/?RSI/75/54/1

[19] A. Luiten, A. Mann, M. Costa, and D. Blair, "Power stabilized cryogenic sapphire oscillator," *IEEE Trans. Instrum. Meas.*, vol. 44, no. 2, pp. 132–135, 1995.

[20] A. Mann, C. Sheng, and A. Luiten, "Cryogenic sapphire oscillator with exceptionally high frequency stability," *IEEE Trans. Instrum. Meas.*, vol. 50, no. 2, pp. 519–521, 2001.

[21] D. Chambon, S. Bize, M. Lours, F. Narbonneau, H. Marion, A. Clairon, G. Santarelli, A. Luiten, and M. Tobar, "Design and realization of a flywheel oscillator for advanced time and frequency metrology," *Rev. Sci. Instrum.*, vol. 76, no. 9, art. no. 094704, 2005.

[22] S. Dawkins, R. Chicireanu, M. Petersen, J. Millo, D. Magalhães, C. Mandache, Y. Le Coq, and S. Bize, "An ultra-stable referenced interrogation system in the deep ultraviolet for a mercury optical lattice clock," *Appl. Phys. B* [Online]. vol. 99, no. 1–2, pp. 41–46, 2010. Available: http://dx.doi.org/10.1007/s00340-009-3830-3

[23] C. Daussy, O. Lopez, A. Amy-Klein, A. Goncharov, M. Guinet, C. Chardonnet, F. Narbonneau, M. Lours, D. Chambon, S. Bize, A. Clairon, G. Santarelli, M. E. Tobar, and A. N. Luiten, "Long-distance frequency dissemination with a resolution of 10^{-17}," *Phys. Rev. Lett.* [Online]. vol. 94, no. 20, art. no. 203904, 2005. Available: http://link.aps.org/abstract/PRL/v94/e203904

[24] J. Hartnett and N. Nand, "Ultra-low vibration pulse-tube cryocooler stabilized cryogenic sapphire oscillator with 10^{-16} fractional frequency stability," *IEEE Trans. Microw. Theory Tech.*, vol. 58, no. 12, pp. 3580–3586, Dec. 2010.

[25] J. Hartnett, N. Nand, C. Wang, and J.-M. Le Floch, "Cryogenic sapphire oscillator using a low-vibration design pulse-tube cryocooler: First results," *IEEE Trans. Ultrason. Ferroelectr. Freq. Control*, vol. 57, no. 5, pp. 1034–1038, May 2010.

[26] S. Grop, P. Y. Bourgeois, N. Bazin, Y. Kersalé, E. Rubiola, C. Langham, M. Oxborrow, D. Clapton, S. Walker, J. D. Vicente, and V. Giordano, "ELISA: A cryocooled 10 GHz oscillator with 10^{-15} frequency stability," *Rev. Sci. Instrum.* [Online]. vol. 81, no. 2, art. no. 025102, 2010. Available: http://link.aip.org/link/?RSI/81/025102/1

[27] S. Grop, V. Giordano, P. Bourgeois, N. Bazin, Y. Kersale, M. Oxborrow, G. Marra, C. Langham, E. Rubiola, and J. DeVincente, "ELISA: An ultra-stable oscillator for ESA deep space antennas," in *IEEE Int. Frequency Control Symp., Joint with the 22nd European Frequency and Time Forum*, 2009, pp. 376–380.

[28] B. Young, F. Cruz, W. Itano, and J. Bergquist, "Visible lasers with subhertz linewidths," *Phys. Rev. Lett.*, vol. 82, no. 19, pp. 3799–3802, 1999.

[29] J. Millo, D. V. Magalhaes, C. Mandache, Y. L. Coq, E. M. L. English, P. G. Westergaard, J. Lodewyck, S. Bize, P. Lemonde, and G. Santarelli, "Ultrastable lasers based on vibration insensitive cavities," *Phys. Rev. A* [Online]. vol. 79, no. 5, art. no. 053829, 2009. Available: http://link.aps.org/abstract/PRA/v79/e053829

[30] Y. Y. Jiang, A. D. Ludlow, N. D. Lemke, R. W. Fox, J. A. Sherman, L.-S. Ma, and C. W. Oates, "Making optical atomic clocks more stable with 10^{-16}-level laser stabilization," *Nat. Photon.* [Online]. vol. 5, no. 3, pp. 158–161, 2011. Available: http://dx.doi.org/10.1038/nphoton.2010.313

[31] B. Lipphardt, G. Grosche, U. Sterr, C. Tamm, S. Weyers, and H. Schnatz, "The stability of an optical clock laser transferred to the interrogation oscillator for a Cs fountain," *IEEE Trans. Instrum. Meas.*, vol. 58, no. 4, pp. 1258–1262, 2008.

[32] J. Millo, R. Boudot, M. Lours, P. Y. Bourgeois, A. N. Luiten, Y. Le Coq, Y. Kersalé, and G. Santarelli, "Ultra-low-noise microwave extraction from fiber-based optical frequency comb," *Opt. Lett.* [Online]. vol. 34, no. 23, pp. 3707–3709, 2009. Available: http://ol.osa.org/abstract.cfm?URI=ol-34-23-3707

[33] J. Millo, M. Abgrall, M. Lours, E. M. L. English, H. Jiang, J. Guéna, A. Clairon, M. E. Tobar, S. Bize, Y. Le Coq, and G. Santarelli, "Ultralow noise microwave generation with fiber-based optical frequency comb and application to atomic fountain clock," *Appl. Phys. Lett.* [Online]. vol. 94, no. 14, art. no. 141105, 2009. Available: http://link.aip.org/link/?APL/94/141105/1

[34] S. Weyers, B. Lipphardt, and H. Schnatz, "Reaching the quantum limit in a fountain clock using a microwave oscillator phase locked to an ultrastable laser," *Phys. Rev. A* [Online]. vol. 79, no. 3, art. no. 031803, 2009. Available: http://link.aps.org/abstract/PRA/v79/e031803

[35] J. Guéna, G. Dudle, and P. Thomann, "An experimental study of intermodulation effects in an atomic fountain frequency standard," *Eur. Phys. J. Appl. Phys.* [Online]. vol. 38, no. 2, pp. 183–189, 2007. Available: http://dx.doi.org/10.1051/epjap:2007072

[36] G. Di Domenico, L. Devenoges, A. Joyet, A. Stefanov, and P. Thomann, "Uncertainty evaluation of the continuous cesium fountain frequency standard FOCS-2," in *Joint Conf. IEEE Int. Frequency Control Symp. and European Frequency and Time Forum*, 2011, pp. 51–55.

[37] R. Li and K. Gibble, "Phase variations in microwave cavities for atomic clocks," *Metrologia* [Online]. vol. 41, no. 6, pp. 376–386, 2004. Available: http://stacks.iop.org/0026-1394/41/376

[38] R. Li and K. Gibble, "Evaluating and minimizing distributed cavity phase errors in atomic clocks," *Metrologia* [Online]. vol. 47, no. 5, pp. 534–551, 2010. Available: http://stacks.iop.org/0026-1394/47/i=5/a=004

[39] J. Guéna, R. Li, K. Gibble, S. Bize, and A. Clairon, "Evaluation of Doppler shifts to improve the accuracy of primary atomic fountain clocks," *Phys. Rev. Lett.*, vol. 106, no. 13, art. no. 130801, Apr. 2011.

[40] R. Li, K. Gibble, and K. Szymaniec, "Improved accuracy of the NPL-CsF2 primary frequency standard: Evaluation of distributed cavity phase and microwave lensing frequency shifts," *Metrologia* [Online]. vol. 48, no. 5, pp. 283–289, 2011. Available: http://stacks.iop.org/0026-1394/48/i=5/a=007

[41] S. Weyers, V. Gerginov, N. Nemitz, R. Li, and K. Gibble, "Distributed cavity phase frequency shifts of the caesium fountain PTB-CSF2," *Metrologia* [Online]. vol. 49, no. 1, pp. 82–87, 2012. Available: http://stacks.iop.org/0026-1394/49/i=1/a=012

[42] J. Guéna, S. Bize, A. Clairon, R. Li, and K. Gibble, "Quantitative evaluation of distributed cavity phase shifts to improve the accuracy of SYRTE FO2," in *Joint Conf. IEEE Int. Frequency Control Symp. and European Frequency and Time Forum*, 2011, pp. 61–62.

[43] P. Wolf and C. J. Bordé, "Recoil effects in microwave Ramsey spectroscopy," [Online]. Available: http://arxiv.org/abs/quant-ph/0403194, 2004.

[44] J. L. Hall, C. J. Bordé, and K. Uehara, "Direct optical resolution of the recoil effect using saturated absorption spectroscopy," *Phys. Rev. Lett.*, vol. 37, no. 20, pp. 1339–1342, 1976.

[45] K. Gibble, "Difference between a photon's momentum and an atom's recoil," *Phys. Rev. Lett.* [Online]. vol. 97, no. 7, art. no. 073002, 2006. Available: http://link.aps.org/abstract/PRL/v97/e073002

[46] W. Itano, L. Lewis, and D. Wineland, "Shift of $^2S_{1/2}$ hyperfine splittings due to blackbody radiation," *Phys. Rev. A*, vol. 25, no. 2, pp. 1233–1235, 1982.

[47] E. Simon, P. Laurent, and A. Clairon, "Measurement of the Stark shift of the Cs hyperfine splitting in an atomic fountain," *Phys. Rev. A*, vol. 57, no. 1, pp. 436–439, 1998.

[48] S. Micalizio, A. Godone, D. Calonico, F. Levi, and L. Lorini, "Blackbody radiation shift of the ^{133}Cs hyperfine transition frequency," *Phys. Rev. A*, vol. 69, no. 5, art. no. 053401, May 2004.

[49] F. Levi, D. Calonico, L. Lorini, S. Micalizio, and A. Godone, "Measurement of the blackbody radiation shift of the ^{133}Cs hyperfine transition in an atomic fountain," *Phys. Rev. A*, vol. 70, no. 3, art. no. 033412, 2004.

[50] A. Godone, D. Calonico, F. Levi, S. Micalizio, and C. Calosso, "Stark-shift measurement of the $^2S_{1/2}$, $F = 3 \rightarrow F = 4$ hyperfine transition of ^{133}Cs," *Phys. Rev. A*, vol. 71, no. 6, art. no. 063401, 2005.

[51] P. Rosenbusch, S. Zhang, and A. Clairon, "Blackbody radiation shift in primary frequency standards," in *IEEE Int. Frequency Control Symp., Joint with the 21st European Frequency and Time Forum*, 2007, pp. 1060–1063.

[52] S. Ulzega, A. Hofer, P. Moroshkin, and A. Weis, "Reconciliation of experimental and theoretical electric tensor polarizabilities of the cesium ground state," *Eur. Phys. Lett.* [Online]. vol. 76, no. 6, pp. 1074–1080, 2006. Available: http://stacks.iop.org/0295-5075/76/i=6/a=1074

[53] P. G. H. Sandars, "Differential polarizability in the ground state of the hydrogen atom," *Proc. Phys. Soc.* [Online]. vol. 92, no. 4, pp. 857–861, 1967. Available: http://stacks.iop.org/0370-1328/92/i=4/a=303

[54] J. R. P. Angel and P. G. H. Sandars, "The hyperfine structure Stark effect. I. Theory," *Proc. R. Soc. London A.* [Online]. vol. 305, no. 1480, pp. 125–138, 1968, Available: http://rspa.royalsocietypublishing.org/content/305/1480/125.abstract

[55] S. Ulzega, A. Hofer, P. Moroshkin, R. Müller-Siebert, D. Nettels, and A. Weis, "Measurement of the forbidden electric tensor polarizability of Cs atoms trapped in solid ^{4}He," *Phys. Rev. A*, vol. 75, no. 4, art. no. 042505, 2007.

[56] E. J. Angstmann, V. A. Dzuba, and V. V. Flambaum, "Frequency shift of the cesium clock transition due to blackbody radiation," *Phys. Rev. Lett.* [Online]. vol. 97, no. 4, art. no. 040802, Jul. 2006. Available: http://link.aps.org/doi/10.1103/PhysRevLett.97.040802

[57] K. Beloy, U. I. Safronova, and A. Derevianko, "High-accuracy calculation of the blackbody radiation shift in the ^{133}Cs primary frequency standard," *Phys. Rev. Lett.*, vol. 97, no. 4, art. no. 040801, 2006.

[58] V. G. Pal'chikov, Y. S. Domnin, and A. V. Novoselov, "Black-body radiation effects and light shifts in atomic frequency standards," *J. Opt. B* [Online]. vol. 5, no. 2, pp. S131–S135, 2003. Available: http://stacks.iop.org/1464-4266/5/i=2/a=370

[59] J. D. Feichtner, M. E. Hoover, and M. Mizushima, "Stark effect of the hyperfine structure of cesium-133," *Phys. Rev.*, vol. 137, no. 3A, pp. A702–A708, Feb. 1965.

[60] T. Lee, T. P. Das, and R. M. Sternheimer, "Perturbation theory for the Stark effect in the hyperfine structure of alkali-metal atoms," *Phys. Rev. A*, vol. 11, no. 6, pp. 1784–1786, Jun. 1975.

[61] J.-L. Robyr, P. Knowles, and A. Weis, "CPT-pump-probe measurement of the Cs clock transition DC Stark shift," in *Joint Conf. IEEE Int. Freq. Control Symp. and European Frequency and Time Forum*, 2011, pp. 1–4.

[62] S. Zhang, "Déplacement de fréquence dû au rayonnement du corps noir dans une fontaine atomique à césium et amélioration des performances de l'horloge," Ph.D. dissertation, Physics Dept., Université Pierre et Marie Curie, Paris VI, Paris, France, 2004, (in French).

[63] T. P. Heavner, T. E. Parker, J. H. Shirley, L. Donley, S. R. Jefferts, F. Levi, D. Calonico, C. Calosso, G. Costanzo, and B. Mongino, "Comparing room temperature and cryogenic cesium fountains," in *Joint Conf. IEEE Int. Frequency Control Symp. and the European Frequency and Time Forum*, 2011, pp. 1–3.

[64] S. Bize, Y. Sortais, M. Santos, C. Mandache, A. Clairon, and C. Salomon, "High-accuracy measurement of the ^{87}Rb ground-state hyperfine splitting in an atomic fountain," *Europhys. Lett.*, vol. 45, no. 5, pp. 558–564, 1999.

[65] E. J. Angstmann, V. A. Dzuba, and V. V. Flambaum, "Frequency shift of hyperfine transitions due to blackbody radiation," *Phys. Rev. A*, vol. 74, no. 2, art. no. 023405, 2006.

[66] M. S. Safronova, D. Jiang, and U. I. Safronova, "Blackbody radiation shift in the ^{87}Rb frequency standard," *Phys. Rev. A*, vol. 82, no. 2, art. no. 022510, 2010.

[67] R. S. S. Weyers and R. Wynands, "Effects of microwave leakage in caesium clocks: Theoretical and experimental results," in *Proc. 2006 European Frequency Time Forum*, 2006.

[68] S. Jefferts, J. Shirley, N. Ashby, T. Heavner, E. Donley, and F. Levi, "On the power dependence of extraneous microwave fields in atomic frequency standards," in *Proc. IEEE Int. Frequency Control Symp. Expo.,* 2005, pp. 105–110.

[69] S. Bize, P. Laurent, M. Abgrall, H. Marion, I. Maksimovic, L. Cacciapuoti, J. Grünert, C. Vian, F. Pereira dos Santos, P. Rosenbusch, P. Lemonde, G. Santarelli, P. Wolf, A. Clairon, A. Luiten, M. Tobar, and C. Salomon, "Advances in ^{133}Cs fountains," *C. R. Phys.*, vol. 5, no. 8, pp. 829–844, 2004.

[70] S. Bize, P. Laurent, M. Abgrall, H. Marion, I. Maksimovic, L. Cacciapuoti, J. Grünert, C. Vian, F. Pereira dos Santos, P. Rosenbusch, P. Lemonde, G. Santarelli, P. Wolf, A. Clairon, A. Luiten, M. Tobar, and C. Salomon, "Cold atom clocks and applications," *J. Phys. B* [Online]. vol. 38, no. 9, pp. S449–S468, 2005. Available: http://stacks.iop.org/0953-4075/38/S449

[71] C. Fertig and K. Gibble, "Measurement and cancellation of the cold collision frequency shift in an ^{87}Rb fountain clock," *Phys. Rev. Lett.*, vol. 85, no. 8, pp. 1622–1625, 2000.

[72] Y. Sortais, S. Bize, C. Nicolas, A. Clairon, C. Salomon, and C. Williams, "Cold collision frequency shifts in a ^{87}Rb fountain," *Phys. Rev. Lett.*, vol. 85, no. 15, pp. 3117–3120, 2000.

[73] S. Bize, Y. Sortais, C. Mandache, A. Clairon, and C. Salomon, "Cavity frequency pulling in cold atom fountains," *IEEE Trans. Instrum. Meas.*, vol. 50, no. 2, pp. 503–506, 2001.

[74] K. Szymaniec, W. Chałupczak, E. Tiesinga, C. J. Williams, S. Weyers, and R. Wynands, "Cancellation of the collisional frequency shift in caesium fountain clocks," *Phys. Rev. Lett.*, vol. 98, no. 15, art. no. 153002, 2007.

[75] K. Szymaniec and S. E. Park, "Primary frequency standard NPL-CsF2: Optimized operation near the collisional shift cancellation point," *IEEE Trans. Instrum. Meas.*, vol. 60, no. 7, pp. 2475–2481, 2011.

[76] W. H. Press, S. A. Teukolsky, W. T. Vetterling, and B. P. Flannery, *Numerical Recipes in C*, 2nd ed., Cambridge, UK: Cambridge University Press, 1992, p. 663. [Online]. Available: http://apps.nrbook.com/c/index.html

[77] T. E. Parker, "Long-term comparison of caesium fountain primary frequency standards," *Metrologia* [Online]. vol. 47, no. 1, pp. 1–10, 2010. Available: http://stacks.iop.org/0026-1394/47/i=1/a=001

[78] H. Marion, F. Pereira Dos Santos, M. Abgrall, S. Zhang, Y. Sortais, S. Bize, I. Maksimovic, D. Calonico, J. Grünert, C. Mandache, P. Lemonde, G. Santarelli, P. Laurent, A. Clairon, and C. Salomon, "Search for variations of fundamental constants using atomic fountain clocks," *Phys. Rev. Lett.*, vol. 90, no. 15, art. no. 150801, 2003.

[79] *Recommendation CCTF-1 2004 Concerning Secondary Representations of the Second.* BIPM-CCTF 2004, 2004, p. 38.

[80] Y. Ovchinnikov and G. Marra, "Accurate rubidium atomic fountain frequency standard," *Metrologia* [Online]. vol. 48, no. 3, p. 87–100, 2011. Available: http://stacks.iop.org/0026-1394/48/i=3/a=003

[81] R. Li and K. Gibble, "Comment on 'accurate rubidium atomic fountain frequency standard'," *Metrologia* [Online]. vol. 48, no. 5, p. 446–447, 2011. Available: http://stacks.iop.org/0026-1394/48/i=5/a=N03

[82] Y. Ovchinnikov and G. Marra, "Reply to comment on 'accurate rubidium atomic fountain frequency standard'," *Metrologia* [Online]. vol. 48, no. 5, pp. 448–449, 2011. Available: http://stacks.iop.org/0026-1394/48/i=5/a=N04

[83] S. Peil, S. Crane, T. Swanson, and C. R. Ekstrom, "The USNO rubidium fountain," in *IEEE Int. Frequency Control Symp. Expo.*, 2006, pp. 304–306.

[84] S. Peil, S. Crane, J. Hanssen, T. B. Swanson, and C. R. Ekstrom, "Measurements with multiple operational fountain clocks," in *Joint Conf. IEEE Int. Frequency Control Symp. and the European Frequency and Time Forum*, 2011, pp. 58–60.

[85] P. Uhrich, D. Valat, and M. Abgrall, "Steering of the French time scale TA(F) towards the LNE-SYRTE primary frequency standards," *Metrologia* [Online]. vol. 45, no. 6, pp. S42–S46, 2008. Available: http://stacks.iop.org/0026-1394/45/i=6/a=S07

[86] C. W. Chou, D. B. Hume, J. C. J. Koelemeij, D. J. Wineland, and T. Rosenband, "Frequency comparison of two high-accuracy Al^+ optical clocks," *Phys. Rev. Lett.*, vol. 104, no. 7, art. no. 070802, Feb. 2010.

[87] N. D. Lemke, A. D. Ludlow, Z. W. Barber, T. M. Fortier, S. A. Diddams, Y. Jiang, S. R. Jefferts, T. P. Heavner, T. E. Parker, and C. W. Oates, "Spin-1/2 optical lattice clock," *Phys. Rev. Lett.* [Online]. vol. 103, no. 6, art. no. 063001, 2009. Available: http://link.aps.org/abstract/PRL/v103/e063001

[88] T. Rosenband, D. B. Hume, P. O. Schmidt, C. W. Chou, A. Brusch, L. Lorini, W. H. Oskay, R. E. Drullinger, T. M. Fortier, J. E. Stalnaker, S. A. Diddams, W. C. Swann, N. R. Newbury, W. M. Itano, D. J. Wineland, and J. C. Bergquist, "Frequency ratio of Al^+ and Hg^+ single-ion optical clocks; Metrology at the 17th decimal place," *Science*, vol. 319, no. 5871, pp. 1808–1812, 2008.

[89] A. D. Ludlow, T. Zelevinsky, G. K. Campbell, S. Blatt, M. M. Boyd, M. H. G. de Miranda, M. J. Martin, J. W. Thomsen, S. M. Foreman, J. Ye, T. M. Fortier, J. E. Stalnaker, S. A. Diddams, Y. L. Coq, Z. W. Barber, N. Poli, N. D. Lemke, K. M. Beck, and C. W. Oates, "Sr lattice clock at 1×10^{-16} fractional uncertainty by remote optical evaluation with a Ca clock," *Science*, vol. 319, no. 5871, pp. 1805–1808, 2008.

[90] Consultative Committee for Time and Frequency (CCTF) Report of the 18th Meeting (June 2009) to the International Committee for Weights and Measures [Online]. Available: http://www.bipm.org/utils/common/pdf/CCTF18.pdf

[91] X. Baillard, M. Fouché, R. L. Targat, P. G. Westergaard, A. Lecallier, F. Chapelet, M. Abgrall, G. D. Rovera, P. Laurent, P. Rosenbusch, S. Bize, G. Santarelli, A. Clairon, P. Lemonde, G. Grosche, B. Lipphardt, and H. Schnatz, "An optical lattice clock with spin-polarized ^{87}Sr atoms," *Eur. Phys. J. D*, vol. 48, no. 1, pp. 11–17, 2008.

[92] S. Blatt, A. D. Ludlow, G. K. Campbell, J. W. Thomsen, T. Zelevinsky, M. M. Boyd, J. Ye, X. Baillard, M. Fouché, R. L. Targat, A. Brusch, P. Lemonde, M. Takamoto, F.-L. Hong, H. Katori, and V. V. Flambaum, "New limits on coupling of fundamental constants to gravity using ^{87}Sr optical lattice clocks," *Phys. Rev. Lett.*, vol. 100, no. 14, art. no. 140801, 2008.

[93] M. Fischer, N. Kolachevsky, M. Zimmermann, R. Holzwarth, T. Udem, T. W. Hänsch, M. Abgrall, J. Grunert, I. Maksimovic, S. Bize, H. Marion, F. P. D. Santos, P. Lemonde, G. Santarelli, P. Laurent, A. Clairon, C. Salomon, M. Haas, U. D. Jentschura, and C. H. Keitel, "New limits on the drift of fundamental constants from laboratory measurements," *Phys. Rev. Lett.*, vol. 92, no. 23, art. no. 230802, 2004.

[94] T. M. Fortier, N. Ashby, J. C. Bergquist, M. J. Delaney, S. A. Diddams, T. P. Heavner, L. Hollberg, W. M. Itano, S. R. Jefferts, K. Kim, F. Levi, L. Lorini, W. H. Oskay, T. E. Parker, J. Shirley, and J. E. Stalnaker, "Precision atomic spectroscopy for improved limits on variation of the fine structure constant and local position invariance," *Phys. Rev. Lett.*, vol. 98, no. 7, art. no. 070801, 2007.

[95] E. Peik, B. Lipphardt, H. Schnatz, T. Schneider, C. Tamm, and S. G. Karshenboim, "Limit on the present temporal variation of the fine structure constant," *Phys. Rev. Lett.*, vol. 93, no. 17, art. no. 170801, 2004.

[96] P. J. Mohr, B. N. Taylor, and D. B. Newell, "CODATA recommended values of the fundamental physical constants: 2006," *Rev. Mod. Phys.* [Online]. vol. 80, no. 2, p. 633–730, 2008. Available: http://link.aps.org/abstract/RMP/v80/p633

[97] S. G. Karshenboim, "Precision physics of simple atoms: QED tests, nuclear structure and fundamental constants," *Phys. Rep.* [Online]. vol. 422, no. 1–2, pp. 1–63, 2005. Available: http://www.sciencedirect.com/science/article/pii/S0370157305003637

[98] M. Niering, R. Holzwarth, J. Reichert, P. Pokasov, T. Udem, M. Weitz, T. W. Hänsch, P. Lemonde, G. Santarelli, M. Abgrall, P. Laurent, C. Salomon, and A. Clairon, "Measurement of the hydrogen 1S–2S transition frequency by phase coherent comparison with a microwave cesium fountain clock," *Phys. Rev. Lett.*, vol. 84, no. 24, pp. 5496–5499, 2000.

[99] C. G. Parthey, A. Matveev, J. Alnis, B. Bernhardt, A. Beyer, R. Holzwarth, A. Maistrou, R. Pohl, K. Predehl, T. Udem, T. Wilken, N. Kolachevsky, M. Abgrall, D. Rovera, C. Salomon, P. Laurent, and T. W. Hänsch, "Improved measurement of the hydrogen 1S–2S transition frequency," *Phys. Rev. Lett.* [Online]. vol. 107, no. 20, art. no. 203001, Nov. 2011. Available: http://link.aps.org/doi/10.1103/PhysRevLett.107.203001

[100] R. Pohl, A. Antognini, F. Nez, F. D. Amaro, F. Biraben, J. M. R. Cardoso, D. S. Covita, A. Dax, S. Dhawan, L. M. P. Fernandes, A. Giesen, T. Graf, T. W. Hänsch, P. Indelicato, L. Julien, C.-Y. Kao, P. Knowles, E.-O. Le Bigot, Y.-W. Liu, J. A. M. Lopes, L. Ludhova, C. M. B. Monteiro, F. Mulhauser, T. Nebel, P. Rabinowitz, J. M. F. dos Santos, L. A. Schaller, K. Schuhmann, C. Schwob, D. Taqqu, J. F. C. A. Veloso, and F. Kottmann, "The size of the proton," *Nature* [Online]. vol. 466, no. 7303, pp. 213–216, Jul. 2010. Available: http://dx.doi.org/10.1038/nature09250

[101] The ALPHA Collaboration, "Confinement of antihydrogen for 1,000 seconds," *Nat. Phys.*, vol. 7, no. 7, pp. 558–564, 2011.

[102] M. Chwalla, J. Benhelm, K. Kim, G. Kirchmair, T. Monz, M. Riebe, P. Schindler, A. S. Villar, W. Hansel, C. F. Roos, R. Blatt, M. Abgrall, G. Santarelli, G. D. Rovera, and P. Laurent, "Absolute frequency measurement of the $^{40}Ca^+$ 4s $^2S_{1/2}$-3d $^2D_{5/2}$ clock transition," *Phys. Rev. Lett.* [Online]. vol. 102, no. 2, art. no. 023002, 2009. Available: http://link.aps.org/abstract/PRL/v102/e023002

[103] X. Baillard, M. Fouché, R. L. Targat, P. G. Westergaard, A. Lecallier, Y. L. Coq, G. D. Rovera, S. Bize, and P. Lemonde, "Accuracy evaluation of an optical lattice clock with bosonic atoms," *Opt. Lett.*, vol. 32, no. 13, pp. 1812–1814, 2007.

[104] R. Le Targat, X. Baillard, M. Fouché, A. Brusch, O. Tcherbakoff, G. D. Rovera, and P. Lemonde, "Accurate optical lattice clock with ^{87}Sr atoms," *Phys. Rev. Lett.*, vol. 97, no. 13, art. no. 130801, 2006.

[105] I. Courtillot, A. Quessada, R. Kovacich, A. Brusch, D. Kolker, J.-J. Zondy, G. Rovera, and P. Lemonde, "Clock transition for a future optical frequency standard with trapped atoms," *Phys. Rev. A*, vol. 68, no. 3, art. no. 030501, 2003.

[106] M. Petersen, R. Chicireanu, S. T. Dawkins, D. V. Magalhaes, C. Mandache, Y. Le Coq, A. Clairon, and S. Bize, "Doppler-free spectroscopy of the $^1S_0$–$^3P_0$ optical clock transition in laser-cooled fermionic isotopes of neutral mercury," *Phys. Rev. Lett.* [Online]. vol. 101, no. 18, art. no. 183004, 2008. Available: http://link.aps.org/abstract/PRL/v101/e183004

[107] L. Yi, S. Mejri, J. J. McFerran, Y. Le Coq, and S. Bize, "Optical lattice trapping of ^{199}Hg and determination of the magic wavelength for the ultraviolet $^1S_0 \leftrightarrow {}^3P_0$ clock transition," *Phys. Rev. Lett.*, vol. 106, no. 7, art. no. 073005, 2011.

[108] P. Laurent, M. Abgrall, C. Jentsch, P. Lemonde, G. Santarelli, A. Clairon, I. Maksimovic, S. Bize, C. Salomon, D. Blonde, J. Vega, O. Grosjean, F. Picard, M. Saccoccio, M. Chaubet, N. Ladiette, L. Guillet, I. Zenone, C. Delaroche, and C. Sirmain, "Design of the cold atom PHARAO space clock and initial test results," *Appl. Phys. B* [Online]. vol. 84, no. 4, pp. 683–690, 2006, Available: http://dx.doi.org/10.1007/s00340-006-2396-6

[109] L. Cacciapuoti, N. Dimarcq, G. Santarelli, P. Laurent, P. Lemonde, A. Clairon, P. Berthoud, A. Jornod, F. Reina, S. Feltham, and C. Salomon, "Atomic clock ensemble in space: Scientific objectives and mission status," *Nucl. Phys. B* [Online]. vol. 166, pp. 303–306, Apr. 2007. Available: http://www.sciencedirect.com/science/article/pii/S0920563206010425

[110] P. Guillemot, E. Samain, P. Vrancken, P. Exertier, and S. Leon, "Time transfer by laser link–T2L2: An opportunity to calibrate RF links," in *Proc. 40th Precise Time and Time Interval Meeting*, 2008, pp. 95–106.

[111] E. Samain, P. Exertier, P. Guillemot, P. Laurent, F. Pierron, D. Rovera, J.-M. Torre, M. Abgrall, J. Achkar, D. Albanese, C. Courde, K. Djeroud, M. L. Bourez, S. Leon, H. Mariey, G. Martinot-Lagarde, J. L. Oneto, J. Paris, M. Pierron, and H. Viot, "Time transfer by laser link–T2L2: Current status and future experiments," in *Joint Conf. IEEE Int. Frequency Control Symp. and the European Frequency and Time Forum*, 2011, pp. 1–6.

[112] G. D. Rovera, M. Abgrall, and P. Laurent, "Contribution to TAI frequency by a travelling primary frequency standard," in *Joint Conf. IEEE Int. Frequency Control and the European Frequency and Time Forum*, 2011, pp. 45–47.

[113] S. G. Karshenboïm, "Some possibilities for laboratory searches for variations of fundamental constants," *Can. J. Phys.*, vol. 78, no. 7, pp. 639–678, 2000.

[114] V. V. Flambaum, "Variation of fundamental constants in space and time: Theory and observations," *Eur. Phys. J.* [Online]. vol. 163, pp. 159–171, Oct. 2008. Available: http://dx.doi.org/10.1140/epjst/e2008-00817-5

[115] J. Uzan, "The fundamental constants and their variation: Observational status and theoretical motivations," *Rev. Mod. Phys.*, vol. 75, no. 2, pp. 403–455, 2003.

[116] J.-P. Uzan, "Varying constants, gravitation and cosmology," *Living Rev. Relativ.*, vol. 14, art. no. 2, 2011. [Online]. Available: http://www.livingreviews.org/lrr-2011-2

[117] J. Guéna, F. Chapelet, P. Rosenbusch, P. Laurent, M. Abgrall, G. Rovera, G. Santarelli, S. Bize, A. Clairon, and M. Tobar, "New measurement of the rubidium hyperfine frequency using LNE-SYRTE fountain ensemble," in *IEEE Int. Frequency Control Symp.*, 2008, pp. 366–370.

[118] V. V. Flambaum, D. B. Leinweber, A. W. Thomas, and R. D. Young, "Limits on variations of the quark masses, QCD scale, and fine structure constant," *Phys. Rev. D*, vol. 69, no. 11, art. no. 115006, Jun. 2004.

[119] V. V. Flambaum and A. F. Tedesco, "Dependence of nuclear magnetic moments on quark masses and limits on temporal variation of fundamental constants from atomic clock experiments," *Phys. Rev. C* [Online]. vol. 73, no. 5, art. no. 055501, 2006. Available: http://link.aps.org/abstract/PRC/v73/e055501

[120] T. Parker and J. Levine, "Impact of new high stability frequency standards on the performance of the NIST AT1 time scale," *IEEE Trans. Ultrason. Ferroelectr. Freq. Control*, vol. 44, no. 6, pp. 1239–1244, Nov. 1997.

[121] N. Ashby, T. P. Heavner, S. R. Jefferts, T. E. Parker, A. G. Radnaev, and Y. O. Dudin, "Testing local position invariance with four cesium-fountain primary frequency standards and four NIST hydrogen masers," *Phys. Rev. Lett.* [Online]. vol. 98, no. 7, art. no. 070802, 2007. Available: http://link.aps.org/abstract/PRL/v98/e070802

[122] C. M. Will, "The confrontation between general relativity and experiment," *Living Rev. Relativ.* [Online]. vol. 9, art. no. 3, 2006. Available: http://www.livingreviews.org/lrr-2006-3

[123] P. Wolf, F. Chapelet, S. Bize, and A. Clairon, "Cold atom clock test of Lorentz invariance in the matter sector," *Phys. Rev. Lett.* [Online]. vol. 96, no. 6, art. no. 060801, 2006. Available: http://link.aps.org/abstract/PRL/v96/e060801

[124] M. E. Tobar, P. Wolf, S. Bize, G. Santarelli, and V. Flambaum, "Testing local Lorentz and position invariance and variation of fundamental constants by searching the derivative of the comparison frequency between a cryogenic sapphire oscillator and hydrogen maser," *Phys. Rev. D Part. Fields Gravit. Cosmol.*, vol. 81, no. 2, art. no. 022003, Jan. 2010.

[125] P. Wolf, S. Bize, A. Clairon, G. Santarelli, M. E. Tobar, and A. N. Luiten, "Improved test of Lorentz invariance in electrodynamics," *Phys. Rev. D Part. Fields Gravit. Cosmol.*, vol. 70, no. 5, art. no. 051902, Sep. 2004.

[126] P. G. Westergaard, J. Lodewyck, L. Lorini, A. Lecallier, E. A. Burt, M. Zawada, J. Millo, and P. Lemonde, "Lattice-induced frequency shifts in Sr optical lattice clocks at the 10^{-17} level," *Phys. Rev. Lett.*, vol. 106, no. 21, art. no. 210801, May 2011.

Authors' photographs and biographies were unavailable at time of publication.